Quartz Fabric Analysis of the Kawishiwi Shear Zone, NE Minnesota

A THESIS
SUMITTED TO THE FACULTY OF THE
UNIVERSITY OF MINNESOTA
BY

CHRISTOPHER GOSCINAK

IN PARTIAL FULFILLMENT OF THE REQUIREMENTS
FOR THE DEGREE OF
MASTER OF SCIENCE

Dr. VICKI HANSEN

MARCH 2014

Acknowledgements

First and foremost I must thank my advisor Dr. Vicki Hansen. From day one Vicki has been supportive in every way and committed to my success not only with this thesis, but with life's numerous obstacles. Put simply, Vicki has taught me how to think critically, problem solve with a level head, and appreciate all the wonder the world and people around you have to offer.

I would also like to extend my appreciation to Dr. John Goodge and Dr. Carlos Carranza-Torres for being on my committee. In particular, I am grateful to John for help with my thesis proposal's introduction. John was kind enough to take time out of his busy schedule to work with me on framing the scientific problem of my thesis. Furthermore, I am grateful to Carlos for providing a valuable outside voice to my committee. Carlos' questions provided an opportunity to view my research from a different perspective resulting in a deeper appreciation of my work.

The Research Instrumentation Laboratory and Dr. Bryan Bandli provided immensely to this thesis. I would not have been able to collect meaningful data were it not for the countless conversations of operating conditions and sample preparation with Bryan.

Fellow graduate student Jon Dyess has been the unofficial 4th member to my committee. With his thought provoking discussions, I have learned how to better communicate science. Thank you, Jon.

Bruce Goetz and Tom Fitz of the Northland College Geoscience Department are credited with my foundation in geology. Their well-crafted courses challenged me and sparked by love for the natural world.

Lastly, I would like to thank my family and friends for their continued support as I worked on this project. During every phone call to Massachusetts, my parents expressed how proud they were of my accomplishments and always encouraged me to work hard and stay positive.

Abstract

Structural fabrics within the Vermilion district, northeastern Minnesota, including metamorphic foliation and elongation lineation (Le), are well established and can be summarized as near-vertical foliation striking northeast containing oblique to vertical Le. The oblique to vertical lineations are present throughout the Vermilion district, yet areas of subhorizontal lineation orientations are also present locally. Despite broad agreement in structural data, first-order interpretations including vorticity axis orientation and shear sense have yet to be agreed upon. Two different interpretations emerge from previous studies: 1) dextral transpression associated with terrane accretion and 2) Le-parallel shearing consisting of regional dip-slip shearing and later, more focused, strike-slip shearing. The Kawishwi Shear Zone (KSZ), one of several Vermilion district shear zones, shows structural relationship particularly well. Foliation consistently strikes east-northeast and dips vertically. Le is broadly down-dip with discrete areas of subhorizontal orientation. Goodman (2008) performed a structural and kinematic analysis of the KSZ and interpreted lineation-parallel shearing with dip-slip shearing followed by strike-slip shearing. However, previous studies do not specifically constrain flow within L-S tectonites relative to Le.

This study aims to characterize the kinematic pattern of flow through use of quartz fabric analysis of *c*- and *a*-axis petrofabrics. The data acquired reveal the dominant slip planes and direction of flow during deformation, and also provide information about deformation temperature and strain geometry. Oriented samples from the KSZ were analyzed by a scanning electron microscope and electron backscatter diffraction (SEM/EBSD) system. Sample KS7J contains a vertical Le and quartz petrofabric data indicate flow nearly parallel to Le, thus dominantly dip-slip displacement. Quartz microstructures are consistent with greenschist-facies deformation. Sample KS6U1, collected from a localized zone with strike-parallel lineation, displays quartz petrofabric data indicative of slip along the prism <*a*> plane with flow parallel to Le. Activation of the higher temperature prism <*a*> plane is attributed to conditions of the quartz vein emplacement. The results of this study support the lineation-parallel shearing hypothesis for deformation within the KSZ. Similar to the results of Goodman (2008), data of this

study support at least two shearing events in the Kawishiwi Shear Zone. Sample KS7J is interpreted to record the pervasive, broad dip-parallel deformation, whereas sample KS6U1 is interpreted to record a late-stage localized strike-parallel deformation. The general shear flow geometry of sample KS7J indicates displacement near-parallel to Le and does not contain a significant strike-parallel component. Data of this study are in line with regional displacement parallel to Le resulting in dominantly vertical movements.

Table of Contents

Acknowledgements……...i
Abstract……ii
Table of Contents……iv
List of Figures……..v
1. Introduction……..……1
2. Background…….……4
2.1 Geologic Setting and Previous Studies of the Vermilion District ...……...4
2.2 Structural Fabric Elements…….……9
3. Methods……..12
3.1 Sample Preparation……..12
3.2 Petrography of Quartz Deformation Mechanisms……...12
3.3 Collection of Quartz Fabric Data…….13
3.4 Coordinate Systems and Scales Used In This Study……...……14
4. Results……...…….15
4.1 Sample KS6U1…….15
4.1.1 Sample KS6U1 Microstructural Observations…….16
4.1.2 Sample KS6U1 SEM/EBSD Operating Conditions…….16
4.1.3 Sample KS6U1 *c*-axis Data……..16
4.1.4 Sample KS6U1 *a*-axis Data……..17
4.2 Sample KS7J……17
4.2.1 Sample KS7J Microstructural Observations…….18
4.2.2 Sample KS7J SEM/EBSD Operating Conditions…….18
4.2.3 Sample KS7J *c*-axis Data……...…18
4.2.4 Sample KS7J *a*-axis Data……..19
4.3 Summary of Results…….19
5. Implications……....21
5.1 Vorticity Vector and Strain Geometry…….……21
5.2 Evaluation of General Shear of Sample KS7J…….……22
5.3 Evaluation of Orthogonal Reactivation Within the KSZ……..23
6. Summary……25
References…...……...……44

List of Figures

Figure 1: Generalized geologic map of the Vermilion District, NE Minnesota……26
Figure 2: Block diagram displaying shear parallel to the elongation lineation…….27
Figure 3: Block diagram displaying dextral transpression hypothesis……..28
Figure 4: Block diagram of S/C fabric geometry of non-coaxial deformation…..29
Figure 5: Deformation mechanisms of quartz and the general microstructures of the recrystallized grains……30
Figure 6: Crystallographic slip systems of quartz……...……..31
Figure 7a: Quartz *c*- and *a*- axes fabrics of various strains states for coaxial deformation…..32
Figure 7b: Quartz *c*-axis fabric symmetry……...32
Figure 8: Electron backscatter pattern of quartz from sample KS7J……...……..33
Figure 9: Stereographic and block diagram displaying the spatial relationship between vorticity axis and elongation lineation……...……..34
Figure 10: Quartz fabrics of sample KS6U1…….……..35
Figure 11: Quartz *c*-axis fabrics of samples KS6U1 and KS7J from Goodman (2008) and this study……36
Figure 12: Photomicrograph of sample KS6U1……..……....37
Figure 13: Photomicrograph of sample KS6U1 outlining SEM/EBSD acquisition area……..38
Figure 14: Quartz fabrics of sample KS7J……...…….…..39
Figure 15: Photomicrograph of sample KS7J..…….……..…….....40
Figure 16: Photomicrograph of sample KS7J outlining SEM/EBSD acquisition area……..…41
Figure 17: Stereographic and block diagram displaying the vorticity axis of the dip-parallel sample KS7J……..……42
Figure 18: Cartoon diagram of the Kawishiwi shear zone……..……..…..43

1. Introduction

The Superior province of northeastern Minnesota contains numerous Archean shear zones. The Kawishiwi, Shagawa Lake, Mud Creek, Murray and Burntside Lake shear zones are identifiable in the field as extensive planar zones of high strain and share similar structural fabrics (Figure 1). Rocks within the shear zones are L-S tectonites and contain a metamorphic foliation and elongation lineation. Foliation is near-vertical and striking east-northeast; elongation lineation ranges from oblique to down-dip, with rare horizontal to subhorizontal orientations (Hudleston et al., 1988; Bauer and Bidwell, 1990; Schultz-Ela and Hudleston, 1991; Goodman, 2008; Karberg, 2009; Johnson, 2009; Erikson, 2010; Goldner, 2013). Despite broad agreement in structural data, first-order interpretations including vorticity axis orientation and shear sense have yet to be agreed upon. Vorticity axis orientation and shear sense interpretations are fundamental to understanding the crustal assembly of the Archean Superior province of northeast Minnesota, which in turn has implications for Archean crustal assembly processes in general.

Archean shear zones of northeast Minnesota have been variably interpreted as recording horizontal, and near-vertical, displacement. Horizontal displacement interpretations originate largely from strain analysis and observations of asymmetric fabrics viewed within sub-horizontal surfaces (Hudleston et al., 1988; Bauer and Bidwell, 1990; Schultz-Ela and Hudleston, 1991). Given the dominant orientation of elongation lineations (oblique to down-dip), these studies call for regional shearing oblique to the elongation lineation at angles ranging from approximately 90° to 45° and they are interpreted to be a result of shortening perpendicular to foliation accompanied by significant strike-slip translation. Conversely, near-vertical displacement interpretations are based on microstructural interpretations of asymmetric kinematic indicators viewed within planes normal to foliation and containing elongation lineation (Goodman, 2008; Karberg, 2009; Johnson, 2009; Erikson, 2010; Goldner, 2013). Asymmetric kinematic indicators were dominantly found within planes normal to foliation and containing elongation lineation, whereas planes normal to foliation and elongation lineation display dominantly symmetric microstructural fabrics. These observations led previous workers

to an interpretation of regional shear parallel to the elongation lineation (dip-parallel or oblique shear). Horizontal and subhorizontal elongation lineations, where present, are interpreted to represent late-stage strike-parallel shear.

Previous interpretations warrant further study for two main reasons. First, ductile flow parameters such as the vorticity axis (a line about which objects rotate during progressive non-coaxial shearing) and slip direction (or slip plane, normal to the vorticity axis) have yet to be specifically constrained for these rocks. Interpretations of horizontal displacements call for the vorticity axis to be oriented at a shallow angle or parallel to dip-parallel elongation lineation. Interpretations of vertical displacements call for the vorticity axis to be at a high angle or normal to dip-parallel elongation lineation. Second, quartz crystallographic preferred orientation analysis can shed light on the orientation of the vorticity axis in L-S tectonites, in addition to providing information on strain-type and flow geometry (Law, 1990 and references therein). With the advent of electron backscatter diffraction, quartz crystallographic data can be collected across a large area within a relatively short time when compared to universal stage measurements on the optical microscope. Another benefit of electron backscatter diffraction is the ability to simultaneously collect both quartz *c*-axis and *a*-axis orientations.

Through the use of quartz crystallographic preferred orientation analysis (herein referred as quartz fabrics), this study attempts to address sample slip direction relative to elongation lineation. Quartz fabric analysis relies on well-established knowledge of how quartz plastically deforms as recorded in the patterns in stereographic projections of *c*- and *a*-axes orientations plotted in relation to foliation and lineation. During progressive deformation, characteristic patterns may emerge. Quartz *c*-axis and *a*-axis pattern geometries are influenced predominantly by deformation temperature and flow geometry (e.g., Lister and Hobbs, 1980; Schmid and Casey, 1986). In this study, pattern geometry resulting from quartz *c*-axis data is used to interpret the governing crystallographic slip plane(s), and pattern geometry resulting from quartz *a*-axis data is used to further constrain slip direction. An interpretation of the orientation of the vorticity axis is made possible by considering both datasets. Additionally, quartz fabric geometry can also

provide an estimate of the relative magnitude of strike-slip and dip-slip components of deformation.

Samples collected from areas of dip-parallel and strike-parallel lineations within the Kawishiwi shear zone were selected due to deformed quartz being present. To aid in constraining deformation temperature, interpretations of characteristic microstructures of deformation mechanisms of quartz (e.g., bulging, subgrain rotation and grain boundary migration; Hirth and Tullis, 1992) are also presented.

2. Background

Prior study of L-S tectonites within the Vermilion district, northeastern Minnesota is divisible into three phases. Early studies (Hooper and Ojkangas, 1971; Sims, 1972, 1976; Hudleston, 1976) focused on large-scale structures, including folds and foliation, that called for flattening due to the emplacement of the Vermilion Granitic Complex located along the northern border of the district and the Giants Range Batholith located along the southern border of the district. Later studies (Hudleston et al., 1988; Schultz-Ela and Hudleston, 1991) performed strain analysis of elongated casts and offered a new interpretation of deformation in the form of dextral transpression with dominant displacement parallel to foliation strike, and normal, or at a high angle to, elongation lineation. Recent studies (Goodman, 2008; Karberg, 2009; Johnson, 2009; Erikson 2010; Goldner, 2013) employed kinematic analysis techniques and presented different interpretations that recognize the importance of ductile shear parallel to elongation lineation. To date, the parameters of vorticity within these L-S tectonites are not well constrained.

2.1 Geologic Setting and Previous Studies of the Vermilion District

The Vermilion district, as first defined by Clements (1903), is a narrow belt of meta-volcanic and meta-sedimentary rocks that extends from the vicinity of Tower, Minnesota northeast to Saganaga Lake and the Canadian border (Figure 1). Located within the Archean Superior Province of the Canadian Shield, the district spans the boundary between the high-grade gneissic Quetico subprovince and the low-grade met*a*-volcanic met*a*-sedimentary, and plutonic units of the Wawa subprovince. Numerous shear zones marked by well-developed L-S tectonites are present throughout the district.

Major units of the district, from oldest to youngest, include the Lower and Upper Ely Greenstone members, the Lake Vermilion Formation, the Knife Lake Formation, and the Newton Lake Formation (Gruner, 1941; Sims, 1972; Sims and Southwick, 1985 and references therein). The Lower and Upper Ely Greenstone include meta-gabbro, meta-diabase, pillowed basalts and cal*c*-alkalic volcanic rocks (Shultz, 1980). The Lake Vermilion Formation is comprised of greywacke and felsic volcanic units (Ojakangas,

1972). Volcanogenic lithic sedimentary units of sandstone, siltstone, conglomerate and slate dominate the Knife Lake group, which also includes hornblende phyric volcanic breccia and tuff (Guner, 1941; Jirsa et al., 2011). The Newton Lake Formation is comprised of mafic meta-igneous rocks including gabbro to diabase basalt flows, clastic volcanic rocks of calc-alkalic and tholieiitic composition, and sedimentary banded iron formation (Shultz, 1980).

Felsic plutonic units intrude the meta-volcanic and meta-sedimentary units to the north and south (Jirsa et al., 2011 and references therein). Plutonic rocks include two major units of the Vermilion Granitic Complex (north) and the Giants Range Batholith (south). The ages of these complexes generally range from 2750 Ma to 2700 Ma (Goldich, 1972 and references therein). The Vermilion Granitic Complex encompasses the local units of granite, tonalite and trondhjemite. The Giants Range Batholith consists of an assemblage of monzonite, quartz monzonite, migmatite and granodiorite.

Rocks containing a metamorphic foliation and elongation lineation are referred to generally as L-S tectonites and are well established in the Vermilion district (Sims, 1972, 1976; Hudleston 1976; Hudleston et al., 1988; Shultz-Ela and Hudelston, 1991; Bauer and Bidwell, 1990; Goodman, 2008; Karberg, 2009; Johnson, 2009; Erikson, 2010). Foliation dominantly strikes east-northeast and is commonly near vertical. Elongation lineation is present within the foliation plane and displays a range in orientation from near horizontal to near vertical and oblique. In this study, pitch is used to describe the orientation of lineation and is defined as the angle from the east side of the horizontal strike of the foliation to the elongation lineation as measure in the foliation plane. Near-horizontal elongation lineations, herein referred to as strike-parallel, have pitch angles of 0°-10° or 180°-170°. Near-vertical elongation lineations, herein referred to as dip-parallel, have pitch angles of 75°-105°. Oblique elongation lineations have pitch angles of 45°-75° and 105°-135°. The Vermilion district is dominated by down-dip elongation lineations with pitch angles of 45°-135°. Shear zones are present throughout the district and are characterized as generally planar zones of L-S tectonites. The Burntside Lake, Shagawa Lake, Kawishiwi, Mud Creek and Murray shear zones cut local units of the district and extend in excess of 20 km in length.

Previous work within the district can be divided into three main approaches on the basis of time and methodology: 1) early macroscopic observations, 2) strain analysis, and 3) recent kinematic microstructural analysis. Early studies focused on macroscopic scale structures, including the orientation of folds and regional foliation (e.g., Hooper and Ojkangas, 1971; Sims, 1972, 1976; Hudleston, 1976). These studies were followed by work employing strain analysis techniques (e.g., Hudleston et al., 1988; Shultz-Ela and Hudleston, 1991). More recent studies focused on kinematic microstructural analysis (e.g., Goodman, 2008; Karberg, 2009; Johnson, 2009; Erikson 2010; Goldner, 2013). Although there is a general agreement with respect to the orientation of structural elements, these studies differ with regard to shear sense interpretations leading to a lively debate with different implications for Archean crustal assembly processes.

Early studies focused on identification of large-scale folds and deformation of the Vermilion district rocks, interpreted to relate to the emplacement of plutonic units (Hooper and Ojkangas, 1971; Sims, 1972, 1976; Hudleston, 1976). Data and interpretation in these studies focused in the area near Tower, Minnesota, along the central and western regions of the district, and are based largely on field relationships. These studies began by identifying cleavage (metamorphic foliation) as near vertical and striking east-northeast. Additional field data included fold axes and lineation orientation. On the basis of fold axis orientation and interlimb-angle, two basic suites of folds were identified, including F_1 folds with horizontal axes and F_2 fold axes that plunge steeply to the east. Additionally, F_1 folds are isoclinal and F_2 folds are open to tight (Hudleston, 1976). The main conclusions of these studies were: 1) north-south directed flattening occurred across the district, and 2) F_1 and F_2 folds formed contemporaneous with emplacement of the plutonic units to the north and south, which squeezed and shortened the region between the plutonic bodies (Hooper and Ojkangas, 1971; Sims, 1972, 1976; Hudleston, 1976).

Hudleston (1976) characterized strain by documenting the shape of elongated clasts within coarse sedimentary units, and offered additional first-order interpretations. Along with areas of flattening, Hudleston (1976) also called for areas of constriction, particularly in the area south of Tower, Minnesota. The major conclusions of this study

were: 1) foliation formed normal to the direction of maximum shortening (Z-axis of the finite strain ellipsoid) and mineral lineation formed parallel to the direction of maximum extension (X axis of the finite strain ellipsoid) and 2) deformation involved lateral shortening and vertical extrusion between the intruding batholiths. This interpretation led to identifying the mineral lineation as an elongation (or stretching) lineation.

The next group of studies focused on detailed observation and strain analysis of flattened and elongated clasts in outcrop (Hudleston et al., 1988; Shultz-Ela and Hudleston, 1991). Field data were consistent with other studies including foliation near vertical and striking east-northeast and lineation pitch values oblique to dip-parallel (45°-135°). The resulting interpretation presented a new model for deformation of the Vermilion district. Along with the lineation representing the direction of maximum extension, these studies called for a different mechanism for flattening and lineation formation. These studies proposed that regional transpression associated with volcanic arc-terrane accretion caused dextral strike-slip shear throughout the district, accompanied by regional compression, all produced by north-northwest directed oblique subduction. Field mapping and outcrop studies by Bauer and Bidwell (1990) and Jirsa et al. (1992) presented similar results and suggested similar interpretations.

Recent studies of the Vermilion district have focused on specific study of the shear zones. The Kawishiwi, Shagawa Lake, Mud Creek, Murray and Burntside Lake shear zones were the subject of detailed field mapping, and microstructural analysis of oriented thin-sections (Goodman, 2008; Erikson 2008, Karberg, 2009; Johnson, 2009; Goldner, 2013). Field mapping reinforced similarities in foliation orientation across the district while also bringing to light local variability in elongation lineation orientation. The Kawishiwi, Shagawa Lake, Mud Creek, Murray and Burntside Lake shear zones are dominated by down-dip elongation lineations of varying pitch. The Kawishiwi, Mud Creek, Murray and Burntside Lake shear zones contain predominately dip-parallel elongation lineations (pitch angles of 75°-105°). The Shagawa Lake shear zone contains dip-parallel and oblique elongation lineations (pitch angles 45°-135°). Localized areas of strike-parallel elongation lineations occur within each shear zone with the exception of

the Murray and Burntside Lake shear zones, which display consistently dip-parallel elongation lineations.

Kinematic analysis employed in this and other recent studies included collecting oriented samples throughout each shear zone and conducting microstructural analysis of these samples. Kinematic interpretations are best made within the plane that displays the greatest degree of asymmetry. This plane, the motion plane, is commonly oriented parallel to the lineation and normal to the foliation, yet this need not be the case in non-plane strain. To constrain the orientation of the motion plane, observations were made in two different planes relative to elongation lineation: 1) the lineation parallel, foliation normal plane and 2) the lineation-normal plane. Asymmetric fabrics in the elongation lineation parallel, foliation normal plane are consistent with lineation-parallel shear, whereas asymmetric fabrics in the lineation normal plane are consistent with shearing at a high angle to the lineation. These studies reveal asymmetric microstructures within the lineation-parallel, foliation normal plane, indicative of lineation-parallel shear (Figure 2). The vorticity axis is interpreted to be at a high angle to the elongation lineation (90°), although it was not explicitly constrained (Goodman, 2008; Karberg, 2009; Johnson, 2009; Erikson 2008; Goldner, 2013).

Major conclusions from recent studies include: 1) widespread shearing occurred parallel to the predominant elongation lineations (down-dip lineations, vertical or near vertical shear) and 2) localized areas containing strike-parallel lineations represent late-stage strike-parallel shear (Goodman, 2008; Karberg, 2009; Johnson, 2009; Erikson 2008). Kinematic interpretations vary only slightly between shear zones. The Kawishiwi and Mud Creek shear zones are interpreted to record areas of both north- and south-side-up shear, followed by localized dextral strike-slip shearing (Goodman, 2008, Karberg, 2009). Similarly, the Shagawa Lake shear zone was interpreted to record both north- and south-side-up shear, followed by localized sinistral strike-slip shear (Erikson, 2008). Johnson (2009) interpreted a deformational history of dip-parallel shear coupled with flattening within the Murray shear zone.

A key question within the Vermilion district relates to the ductile flow within the region's shear zones, and in particular, the orientation of the vorticity axis relative to the

elongation lineation. Although previous studies demonstrate that the elongation lineations represent the direction of maximum extension (or stretching), the relationship between flow direction and lineation has yet to be robustly established. Given the down-dip orientation of the elongation lineation, dextral transpression interpretations invoke ductile flow at varying angles to the elongation lineation, ranging from 90° (dip-parallel lineations) to 45° (oblique lineations) to 0° (strike-parallel lineations) (Figure 3). Recent studies invoke flow parallel to the elongation lineation, regardless of lineation orientation (Figure 2).

2.2 Structural Fabric Elements

Structural fabric data in this study include features recognized in the field such as foliation and elongation lineation, kinematic microstructures such as S/C foliations and rotated grains, microstructures characteristic of quartz recrystallization mechanisms, and crystallographic fabric elements documented by a scanning electron microscope using an electron backscatter diffraction system.

Metamorphic foliations (Mf) are planar features that occur penetratively throughout the rock. Two types of discrete foliations, S and C, commonly develop during non-coaxial shear (Berthé et al., 1979; Lister and Snoke, 1984). S-foliation surfaces are continuous cleavages commonly marked by grain-shape preferred-orientations of quartz aggregates and are related to the accumulation of finite strain. C-foliation surfaces, commonly marked by mica, cut S-surfaces and are discontinuous discrete planes that represent high shear strain. C-surfaces parallel shear zone boundaries; the relative orientation of C- and S- surfaces is a strong indicator of shear direction (Figure 4) (Berthé et al., 1979; Lister and Snoke, 1984).

Elongation lineations (Le) are linear features that occur penetratively throughout a rock as a result of elongation or stretching during deformation. Le can further be classified based on the foliation plane containing the lineation. Lineations present on S-surfaces are termed Ls whereas lineations present on C-surfaces are termed Lc. Although both Ls and Lc are formed as a result of stretching, Lc are a direct consequence of shearing rather than accumulation of strain; as such, Lc lineations provide the best

indicator of shear (Lin and Williams, 1992; Lin et al., 2007). Lc, unlike Ls, lies within the shear plane, and is therefore parallel to the displacement direction. Recognition of Ls versus Lc may be possible by careful field observation. In addition to identifying S- and C-surfaces in the field, Lc typically present a ridge-and-groove morphology on C-surfaces.

Quartz petrofabrics record operative deformation mechanisms, which can in turn provide general deformation temperature constraints. Recrystallization mechanisms of quartz are dependent primarily on temperature, based on experimentally and naturally deformed samples and average geologic strain rates (Hirth and Tullis, 1992; Stipp et al., 2002). Recrystallization mechanisms of quartz consist of grain-boundary bulging, subgrain rotation and grain-boundary migration (Figure 5) (Drury et al., 1985; Shigematsu, 1999; Stipp et al., 2002). At low temperature, grain boundary mobility is low and boundary movement occurs locally. Recrystallization occurs when the grain boundary bulges into an adjacent grain of high dislocation density, commonly along the boundaries of old grains and triple junctures (Drury et al., 1985; Shigematsu, 1999; Stipp et al., 2002). This process of bulging generally occurs at 270-390 °C, transitioning to subgrain rotation at 390-410 °C. Subgrain rotation recrystallization is characterized by subgrains progressively rotating in response to migration of dislocations into subgrain walls leading to the formation of new grains. Subgrain rotation is dominant at temperatures of 410-490 °C and transitions to grain-boundary migration at 490-520 °C. At high temperatures (greater than 520 °C), grain-boundary mobility is high and grain boundaries migrate easily and engulf entire crystals.

A common phenomenon of ductile deformation is the formation of a crystallographic preferred orientation (CPO). CPO is commonly represented using stereographic projections of crystallographic axis orientations plotted relative to foliation and elongation lineation. Fabric maxima, girdles and skeletons are descriptive terms of fabric geometry. Maximas occur in areas of relatively high concentration of points. Fabric girdles are simply the best-fit great or small circles for any given set of points on a stereonet, and fabric skeletons are constructed of lines that connect individual maximas.

Quartz *a*- and *c*-axis fabric plots commonly contain characteristic patterns governed by temperature, non-coaxiality of flow, and strain geometry (Lister and Hobbs, 1980; Schmid and Casey, 1986; Law, 1990). Quartz fabric plots are useful in determining the deformation symmetry or asymmetry, active slip-system, vorticity, and flow direction during deformation. The major slip-systems of quartz with increasing activation temperature are basal <*a*>, rhombic <*a*>, prism <*a*> and prism <*c*> (Figure 6). Typical *c*-axis patterns of coaxial plane-strain deformation (pure shear) consist of two small-circle girdles connected with a great-circle girdle (Type I crossed girdle). *C*-axis patterns typical of constriction contain two great circle girdles whereas *c*-axis patterns typical of flattening contain two small circle girdles (Figure 7). Fabric patterns resulting from plane-strain deformation consist of two small circle girdles connected with a great circle girdle (Type I crossed girdle).

Shear sense and flow direction interpretation is possible by considering the fabric symmetry and active slip systems. Symmetric quartz *c*-axis and *a*-axis fabrics are representative of coaxial deformation, whereas asymmetric fabrics are representative of non-coaxial deformation (Lister & Hobbs, 1980; Schmid & Casey, 1986). As previously mentioned, the vorticity axis can be represented as a line about which objects rotate. In non-coaxial plane-strain, the vorticity axis is parallel to the Y-axis of the finite strain ellipsoid. Similarly, in coaxial plane-strain deformation (pure shear), the vorticity axis is parallel to the Y-axis of the finite strain ellipsoid, yet there is not a preferred direction of vorticity. Both quartz *c*-axis and *a*-axis fabric data provide information on the orientation of the vorticity axis. *C*-axes fabric skeletons tend to rotate towards the foliation in the direction of shear (Figure 7b). This rotation tracks vorticity and can be interpreted to be the vorticity axis. Issues may arise when only considering *c*-axis fabrics for vorticity axis interpretations, mainly due to more complex flow geometries resulting in less interpretable fabrics. An interpretation of the vorticity axis using *a*-axis fabrics relies on the assumption of slip in the direction of an *a*-axis. This assumption is valid where prism <*c*> is not an active slip system (i.e., at low to medium-high temperatures of shear). Because the basal <*a*>, rhomb <*a*> or prism <*a*> planes accommodate slip in the direction of one of the *a*-axes, the plane containing the *a*-axis maxima (*a*-axis maxima girdle) is interpreted to be the dominant slip plane. In non-coaxial deformation, the

vorticity axis is normal to the dominant slip plane, leading to an interpretation that the pole to the *a*-axis maxima girdle is the vorticity axis.

3. Methods

The objective of this study is to gain insight on the character of ductile flow within the L-S tectonites of the Kawishiwi shear zone. Sample orientation was tracked throughout the study. Petrography was performed to distinguish microstructures interpreted to be the result of different deformation mechanisms. Quartz fabric data were acquired using the SEM/EBSD at the University of Minnesota Duluth (UMD) Research Instrumentation Laboratory. The primary goal during data collection using the SEM/EBSD was to examine a large sample area in a timely manner without sacrificing electron backscatter pattern quality. Samples collected from areas of dip-parallel and strike-parallel lineations were selected due to deformed quartz being present.

3.1 Sample Preparation

Two main goals of sample preparation in this study are: 1) preserving sample orientation and 2) polishing thin-section surfaces to a quality sufficient for SEM/EBSD. Collecting oriented samples in the field and tracking the orientation throughout the thin-sectioning process is vital to correctly identifying shear sense with respect to map structures. Sample collection and sectioning followed the procedure of Hansen (1990). During thin-sectioning, marks were cut on the corner of the thin-section chip enabling reconstruction of sample orientation. Samples were sectioned at a commercial lab and underwent microprobe polish. Upon receiving the thin-section, sample orientation was confirmed by examining the remaining billet and hand sample. Additional polish was applied through use of a colloidal silica bath for three hours. Samples were not subjected to a conductive coating prior to SEM/EBSD analysis.

3.2 Petrography of Quartz Deformation Mechanisms

Thin-sections were examined by optical petrography and microstructures interpreted to be the result of deformation mechanisms (bulging, subgrain rotation, and grain-boundary migration) were documented. As previously mentioned, the active deformation mechanism during deformation provides general temperature constraints.

Bulging microstructures include relatively large grains displaying undulose extinction and defined subdomains with smaller grains present along grain boundaries. Large grains are interpreted to represent relic grains, whereas small grains represent new grains forming by bulging. Unlike bulging, grains recrystallized by subgrain rotation typically display uniform grain size. Additionally, a grain-shape-preferred orientation is commonly present. Grains recrystallized as a result of grain-boundary migration display variability of grain size and irregular grain boundaries.

3.3 Collection of Quartz Fabric Data

Orientations of quartz *c*- and *a*-axes were obtained by SEM/EBSD. SEM/EBSD operates by imaging and indexing electron backscatter patterns (EBSP), a phenomena created through the interaction of the electron beam and the lattice planes of the crystalline material. EBSPs contain Kikuchi bands representative of sample orientation. Kikuchi bands are generated when backscattered electrons diffract through lattice planes and collide with a phosphor screen (Figure 8). The resulting image is captured by a charged-coupled camera and sent to a computer for indexing. Indexing occurs when the software matches the EBSP with known standards. This results in identification of phase and orientation. Mean angular deviation values (MAD) are one way to quantify how well observed and expected EBSPs match. MAD values are expressed as the average angular misfit between the observed and expected Kikuchi bands. In this study, acceptable MAD values were limited to less than 1 degree.

The SEM at UMD is equipped with a HKL EBSD detector and the Channel 5 software suite. The program Flamenco® is used to collect EBSD data. This is achieved through interactive and automated processes. Interactive data collection consists of the user controlling all aspects of the SEM and Flamenco® throughout the collection process. The operator manually chooses the acquisition sites (typically in reference to an orientation contrast image) and moves the stage accordingly. Alternatively, automated data collection consists of Flamenco® determining the acquisition sites and stage movements based on parameters defined by the operator. Parameters of automated data collection broadly include defining the spatial limits, number and location of acquisition

sites in addition to various parameters involved in the indexing of EBSD patterns. These parameters remain constant throughout an automated data collection session.

Data collection for this study used automated techniques, wherein the stage moved a specified distance between each acquisition point. This distance, the step size, is ultimately tied to grain-size. The average grain-size was determined petrographically for each sample. In this way, the SEM/EBSD mimics universal stage methodology where each grain represents a single data point. In practice, however, grains larger than the average grain size may be indexed multiple times.

3.4 Coordinate Systems and Scales Used In This Study

Three main coordinate systems were used in this study: 1) geographic, 2) macroscopic structural features, and 3) crystallographic. Geographic coordinates consist of map-scale observations and interpretations with respect to north. At this scale, observations include broad foliation (i.e., no distinction between S- and C- surfaces), and interpretations include shear-sense (i.e., north- or south- side up, dextral, sinistral). A more focused coordinate system employs the macroscopic fabric, foliation and lineation, as reference. In this case, the type of foliation (i.e., S or C) and elongation lineation (i.e., Ls or Lc) are noted. Interpretations at this scale include shear-sense based on asymmetries of S/C surfaces, vorticity relative to the lineation, and orientation of the motion plane. Lastly, the crystallographic coordinate system uses the orientations of quartz *c*- and *a*-axes leading to observations of fabric pattern geometry and interpretation of active slip systems during deformation.

In this study I use the term vorticity profile plane (VPP) when referring to the motion plane in crystallographic coordinates. When using VPP, I imply the orientation was determined using quartz *c*-axis or *a*-axis data rather than macroscopic structural features.

4. Results

Two samples, KS6U1 and KS7J, were the focus of this study because they sample deformed quartz, which displays a strong crystallographic preferred orientation when viewed with an optical microscope. Quartz fabrics from this study directly address the orientation of the vorticity axis in relation to Le (Figure 9). Sample KS6U1, a sample from a localized shear zone, contains a strike-parallel Le and displays fabric geometry interpreted to be a result of late-stage right-lateral monoclinic simple shear (Goodman, 2008). Quartz *c*-axis fabric data from this study support data from Goodman (2008) and indicates sample KS6U1 underwent shear parallel to Le with a vorticity axis normal to Le, contained within Mf. Quartz *a*-axis data from this study also suggests right-lateral monoclinic simple shear with the vorticity axis normal to Le.

Sample KS7J contains a dip-parallel lineation representative of the KSZ and displays S/C fabrics interpreted to be a result of non-coaxial shearing with north-side up shear sense (Goodman, 2008). Quartz *c*-axis fabric data from this study grossly mimic data from Goodman (2008). Data of this study display more complex patterns suggestive of non-plane strain. *C*-axis data from this study indicate sample KS7J records general shear with the vorticity axis nearly perpendicular to Le and shear direction near parallel to Le.

These two samples are discussed in detail below.

4.1 Sample KS6U1

Sample KS6U1 is consist of deformed quartz vein material with a strike-parallel Le. Strike-parallel Le is localized and the surrounding host rocks display a dip-parallel Le. Mf orientation remains similar within the localized zone. The quartz vein itself parallels Mf oriented 285, 80N. Microstructures including triple-junctures, undulose extinction, and well-defined boundaries indicate that the sample experienced subgrain rotation recrystallization. Quartz crystallographic fabrics display a well-defined pattern indicative of monoclinic plane-strain non-coaxial shear (simple shear) (Figure 10). *C*-axis data are consistent with universal stage data of Goodman (2008), which displays evidence for prism <*a*> slip (Figure 11). Both *c*- and *a*-axis data suggest similar

orientations of the dominant slip plane and the vorticity axis. The dominant slip plane is also consistent with S/C fabrics of right-lateral shear. The vorticity axis is oriented normal to Le and contained within Mf.

4.1.1 Sample KS6U1 Microstructural Observations

Microstructures of sample KS6U1 display asymmetry within an Le-normal Mf-normal plane and the Le-parallel, Mf-normal plane (Goodman, 2008). Individual quartz grains are roughly 250 micrometers. Quartz grains display triple-junctures, undulose extinction, and well-defined boundaries (Figure 12). Inclusions within quartz are generally not present. These observations indicate that quartz within sample KS6U1 underwent subgrain rotation recrystallization. This corresponds to regime II of Hirth and Tullis (1992) and indicates deformation temperatures ranging from 390 to 490 °C (Stipp et al., 2002). The presence of quartz subgrains, deformation fractures within feldspar, and lack of high-temperature minerals such as amphibole may indicate deformation temperatures were closer to the lower end of the range between 390-490 °C.

4.1.2 Sample KS6U1 SEM/EBSD Operating Conditions

Quartz *c*- and *a*- axis fabric data were acquired from a Le-normal plane; data were rotated for display into a Le-parallel Mf-normal plane. SEM/EBSD operating conditions included a Hough resolution of 80, 70 reflectors, 2x2 binning, beam current of 15Kv, and a chamber pressure of 1Pa. Of the 2100 acquisition sites, 1726 produced quartz EBSPs suitable for indexing (MAD values less than 1). Sample step size was equal to the average grain size, 246 micrometers. A total area of 1.27 cm^2 was analyzed (Figure 13).

4.1.3 Sample KS6U1 *c*-axis Data

Sample KS6U1 *c*-axis data display a single girdle containing populations associated with the prism <*a*> slip system (Figure 10). Normal to the *c*-axis girdle is the dominant slip plane (*C*-plane). The asymmetry of the girdle is best displayed by the fabric skeleton and is consistent with right-lateral shearing (Figure 10). This asymmetry indicates that the vorticity axis is normal to Le, contained within the S-foliation plane.

4.1.4 Sample KS6U1 *a*-axis Data

Sample KS6U1 *a*-axis data display a girdle of maxima located along the great circle when viewed in an Ls-parallel Mf-normal plane (Figure 10). This is consistent with plane-strain deformation. The orientation of the slip plane and vorticity axis can be determined by considering the active slip systems. With the exception of prism <*c*> slip, all other slip planes act in the direction of an *a*-axis. Thus, at low to medium-high temperatures, where basal <*a*>, rhomb <*a*> or prism <*a*> planes accommodate slip, *a*-axis populations tend to cluster around the dominant slip direction. The two maxima lie within the C-plane, indicating this is the slip plane (Figure 10). Furthermore, one would expect to find asymmetry viewed in a plane normal to the slip plane and normal to the slip direction in that plane (*a*-axis maxima girdle). Thus, in quartz crystallographic coordinates, the *a*-axis maxima girdle is analogous to the VPP. Furthermore, the pole to the *a*-axis maxima girdle is the vorticity axis (Figure 10B).

4.2 Sample KS7J

Sample KS7J is characterized by deformed quartz vein material with a dip-parallel Le. Surrounding host rocks also contain a dip-parallel Le and Mf is near vertical. Quartz fabric pattern geometry is indicative of general shear with displacement oriented near parallel to Le (Figure 14). *C*-axis data are consistent with universal stage data of Goodman (2008), displaying basal <*a*>, rhomb <*a*> +/- prism <*a*> slip (Figure 11B) with right lateral asymmetry. The right-lateral asymmetry corresponds to north-side-up shear sense in geographic coordinates. The *a*-axis maxima girdle is not oriented along the great circle within an Le-parallel, Mf-normal plane, indicating that the deformation was likely by general shear flow, rather than simple shear. The pole to the *a*-axis maxima girdle, interpreted as the vorticity axis, is located near 90 degrees from Le. Viewed looking down Le, *c*- and *a*-axis data display symmetric fabrics further establishing that the orientation of the vorticity axis is nearly 90 degrees from the Le rather than parallel or near parallel to Le.

4.2.1 Sample KS7J Microstructural Observations

Microstructures of sample KS7J display asymmetries within an Ls-parallel, Mf-normal plane (Goodman, 2008). Quartz grains display a range of grain size from 50-1000 micrometers, with an average grain size of roughly 500 micrometers. Quartz grains display well-defined subgrains, undulose extinction, and diffuse boundaries (Figure 15). Inclusions within quartz are generally not present. These observations indicate sample KS7J underwent bulging recrystallization. This corresponds to regime I of Hirth and Tullis (1992) and indicates deformation temperatures ranging from 270°C - 390°C (Stipp et al., 2002).

4.2.2 Sample KS7J SEM/EBSD Operating Conditions

Quartz *c*- and *a*- axis fabric data was acquired from a Ls-parallel Mf-normal plane; data were rotated for display into three other planes: 1) plotting the fabric in relation to the S-plane, 2) looking down the pole to the *a*-axis maxima girdle, and 3) looking down Le (Figure 14). SEM/EBSD operating conditions included a Hough resolution of 80, 70 reflectors, 2x2 binning, beam current of 15Kv, and a chamber pressure of 1Pa. Of the 980 acquisition sites, 676 produced quartz EBSPs suitable for indexing (MAD values less than 1). Sample step size was equal to the average grain size, 500 micrometers. A total area of 2.45 cm^2 was analyzed (Figure 16).

4.2.3 Sample KS7J *c*-axis Data

Sample KS7J quartz *c*-axis data display populations associated with the basal <*a*>, rhomb <*a*> +/-prism <*a*> slip systems (Figure 14A.i). Normal to the *c*-axis girdle is the dominant slip plane (C-plane). The orientation of the S-plane is marked by a grain-shape-preferred orientation of quartz in thin-section. *C*-axis fabric displays right-lateral asymmetry (Figure 14B.i). The right-lateral sense of shear corresponds to north-side-up in geographic coordinates. *C*-axis fabric grossly mimics data of Goodman (2008) (Figure 11B). Goodman (2008) interpreted the vorticity axis to be oriented normal to Ls based on the inclined *c*-axis fabric. This orientation of vorticity is somewhat supported by quartz *c*-axis data of this study, yet taken without *a*-axis data it is difficult to state with certainty. To test if the vorticity axis is at this orientation, *c*-axis data was rotated into a VPP

(rotation based on *a*-axis data). Within a VPP (Figure 14C.i), right-lateral asymmetry is present, suggesting the vorticity axis could be located 90 ± 20 degrees from Ls. To test if vorticity is parallel to Le, fabric data were rotated to be viewed looking down Le. Within this view, *c*-axis fabrics display symmetry indicating the vorticity axis is not parallel to Ls (Figure 14D.i).

4.2.4 Sample KS7J *a*-axes Data

Sample KS7J quartz *a*-axis fabric geometry displays a maxima girdle oriented oblique to the great circle in a Le-parallel Mf-normal plane (Figures 14B.i and 14B.ii). This fabric is indicative of non-coaxial non-plane-strain shear, or general shear. Furthermore, the *a*-axis maxima all have similar contour values, leading to complexity in determining the dominant slip plane. The similarity in the contour values of *a*-axis maxims is possibly due to the flow geometry of general shear wherein slip occurs at relatively similar amounts in each *a*-axis direction (the influence of the coaxial component of deformation). As discussed earlier, the pole to the *a*-axis maxima girdle is interpreted to be the vorticity axis. Sample KS7J displays a vorticity axis oriented near 90 (± 20) degrees from Le (Figures 9 and 17).

4.3 Summary of Results

The major results of this study are:

1. Sample KS6U1 with a strike-parallel Le, records dextral simple-shear wherein displacement was parallel to Le and the vorticity axis is contained in Mf and perpendicular to Le.
2. Deformation temperature of sample KS6U1 was determined by interpreting microstructures thought to be the result of subgrain rotation recrystallization at 390-490 °C.
3. Sample KS7J with a dip-parallel Le, represents general shear wherein displacement was near parallel to Le and the vorticity axis is not contained in Mf, although oriented near perpendicular to Le.

4. Deformation temperature of sample KS7J was determined by interpreting microstructures thought to be the result of boundary bulging recrystallization at 270-390 °C.
5. The data presented here support the two-stage history of the Kawishiwi shear zone as proposed by Goodman (2008), in which broadly developed dip-slip deformation predated later-stage localized strike-slip deformation.
6. Later-stage strike-parallel shear was localized within a narrow quartz vein and microstructures relate relatively higher deformation temperature to the vein environment.

5. Implications

The results of this study support the Le-parallel shearing hypothesis for deformation within the Kawishiwi shear zone. Non-coaxial shear was found to be parallel to the strike-parallel Le of sample KS6U1 and near parallel to the dip-parallel Le of sample KS7J. The vorticity vector was determined to be contained in Mf and perpendicular to Le in sample KS6U1. The vorticity vector was determined to not be contained in Mf, but lie in a plane with a similar orientation and near perpendicular to Le in sample KS7J. Similar to the results of Goodman (2008), data of this study support at least two shearing events in the Kawishiwi shear zone. Sample KS7J is interpreted to represent the board dip-parallel deformation and records displacement near parallel to Le. Sample KS6U1 is interpreted to represent the later-stage localized strike-parallel deformation. The general shear flow geometry of sample KS7J does not contain a significant strike-parallel component.

Sample KS6U1 is interpreted to represent a later-stage, localized, strike-parallel deformation at a higher temperature than the initial, broadly developed, dip-parallel deformation recorded by sample KS7J. This interpretation is supported by relationships in the field and microstructural observations. It is important to note that the KSZ is dominated by dip-parallel Le. Strike-parallel Le is present only locally in discrete, narrow domains (Figure 18). The quartz vein that KS6U1 samples is sharply bounded by areas of dip-parallel Le. Microstructures consistent with subgrain rotation recrystallization are typified in sample KS6U1 and along with quartz fabrics suggest the vein was warmer than the host rock during deformation. Further study of this interaction may shed light on the vein fluids and possibly have implications for gold mineralization.

5.1 Vorticity Vector and Strain Geometry

The results of this study identify the vorticity vector within the Kawishiwi shear zone of northeastern Minnesota. Previous studies call for varying orientations of the vorticity axis relative to Le. Interpretations of lineation-parallel shearing call for the vorticity axis to be contained within Mf and oriented normal to Le (Figure 2) (e.g., Goodman, 2008; Erikson, 2008; Karberg, 2009; Johnson, 2009; Goldner, 2013), whereas

interpretations of horizontal displacements call for the vorticity axis to be oriented normal to the horizontal (parallel to dip-parallel Le) (Figure 3) (e.g., Hudleston et al., 1988; Shultz-Ela and Hudleston, 1991). Two samples KS6U1 and KS7J were analyzed containing a strike-parallel and dip-parallel Le, respectively. Within the Kawishiwi shear zone, dip-parallel Le dominates. Quartz crystallographic fabric data from sample KS6U1 indicate a vorticity vector contained within Mf and oriented 90° from the Le (Figure 10). Fabric geometry and asymmetry further indicate plane-strain non-coaxial shear (e.g. simple shear) parallel to Le. Quartz fabric data from sample KS7J indicate the vorticity vector is not contained in Mf, but lies in a plane with a similar orientation and near perpendicular to Le (Figures 14 and 17). Fabric geometry and asymmetry further indicate non-coaxial non-plane-strain shear (general shear).

Both samples indicate conditions consistent with Le-parallel shear. Quartz crystallographic fabrics of sample KS6U1 display a well-defined pattern indicative of monoclinic plane-strain non-coaxial shear (simple shear) (Figure 10). Both *c*- and *a*-axis data suggest similar orientations of the dominant slip plane and the vorticity axis. The dominant slip plane is also consistent with S/C fabrics of right lateral shear. The vorticity axis is oriented normal to Le and contained within Mf. Quartz crystallographic fabrics of sample KS7J indicate general shear with displacement oriented near parallel to Le (Figure 14). The *a*-axis maxima girdle is not oriented along the great circle within an Le-parallel, Mf-normal plane indicating that the deformation was likely general shear flow geometry, rather than plane-strain. The vorticity axis does not lie in Mf, but in a plane with a similar orientation and near perpendicular to Le. Fabrics viewed looking down Le display symmetric fabrics further establishing that the orientation of the vorticity axis is nearly 90 degrees from the Le rather than parallel or near parallel to Le.

5.2 Evaluation of General Shear of Sample KS7J

Sample KS7J displays quartz fabrics interpreted to be a result of general shear. Further evaluation is warranted as previous studies called for general shear flow geometries with a significant strike-parallel component (e.g., transpression; Hudleston et al., 1988; Shultz-Ela and Hudleston, 1991). Quartz fabrics of sample KS7J discount a significant strike-parallel component for two main reasons. First, asymmetric fabrics are

present within a Le-parallel Mf normal plane indicative non-coaxial shear (Figures 14). Fabric geometry is consistent with shear near parallel to Le (near vertical in geographic coordinates). Second, symmetric fabrics are present within a Le-normal plane (Figure 14d). Because the Le is oriented parallel to the dip of the foliation (near vertical in geographic space), a significant strike-parallel component would lead to an asymmetric fabric within a plane normal to the lineation. These symmetric fabrics, in addition to the orientation of vorticity axis, together are inconsistent with a significant strike-parallel component of general shear within sample KS7J.

5.3 Evaluation of Orthogonal Reactivation Within the KSZ

Goodman (2008) first identified the presence of the medium-high temperature prism <*a*> slip system in the relatively low temperature host rock of the KSZ and suggested orthogonal reactivation as a candidate to explain this phenomena. Orthogonal reactivation is a hypothesis presented by Oliver (1996) to account for apparent high-temperature slip at low temperature due to shearing in two orthogonal directions. In this scenario, initial non-coaxial shear would produce a crystallographic preferred orientation within quartz; subsequent orthogonal shear would exploit weaknesses within the aligned quartz lattice and trigger slip along high-temperature slip planes. Oliver (1996) argued that *a*-axes provide a possible test for this model. Given an X-Y-Z coordinate system where X is the lineation, Z is the pole to the foliation and Y is perpendicular to X and Z, orthogonal reactivation calls for *a*-axis maxima contained within the YZ plane. Sample KS6U1 contains *a*-axis maxima within the XZ plane, thus discrediting the idea that orthogonal reactivation led to the formation of quartz fabric patterns in the KSZ strike-parallel sample. Furthermore, microstructures are interpreted to represent subgrain rotation recrystallization at temperatures of 390-490 °C. These two factors taken together are perhaps best interpreted as indicating that the prism <*a*> slip is representative of medium-high deformation temperature within the quartz of sample KS6U1.

5.4 Limitations of This Study and Suggestions for Future Work

The results of this study apply only to the Kawishiwi shear zone. However, only two samples were analyzed and interpretations for the remainder of the Vermilion district

are not made. Additionally, this analysis relies heavily on quartz *a*-axis fabrics in determining the vorticity profile plane and the vorticity vector. Although the effects of general shear on *c*-axis fabric geometry are well established (e.g. changes to fabric symmetry), it is much less clear what response general shear has on *a*-axis fabric geometry. Future work within the Vermilion district could entail analyzing samples from other shear zones to gain regional insight. Analyzing quartz *a*-axis fabrics within more complex shear zones such as transpressional, transtensional or stretching faults may provide knowledge of the influence of non-plane-strain flow on fabric geometry.

6. Summary

Archean shear zones of northeastern Minnesota have been variably interpreted as evidence for horizontal and near-vertical displacement. Through the use of quartz crystallographic preferred orientations analysis this study attempts to address sample slip direction relative to mineral elongation lineation. Samples collected from areas of dip-parallel and strike-parallel Le within the Kawishiwi shear zone were selected due to deformed quartz being present. The results of this study support the lineation-parallel shearing hypothesis for deformation within the Kawishiwi shear zone. Similar to the results of Goodman (2008), data of this study support at least two shearing events in the Kawishiwi shear zone. Sample KS7J is interpreted to record the pervasive, broad dip-parallel deformation whereas sample KS6U1 is interpreted to record a late-stage localized strike-parallel deformation. The general shear flow geometry of sample KS7J indicates displacement near parallel to Le and does not contain a significant strike-parallel component.

Figure 1. Generalized geologic map, annotated with previous studies, of the Vermilion Distrcit, NE Minnesota. Geology from Jirsa et al. 2011.

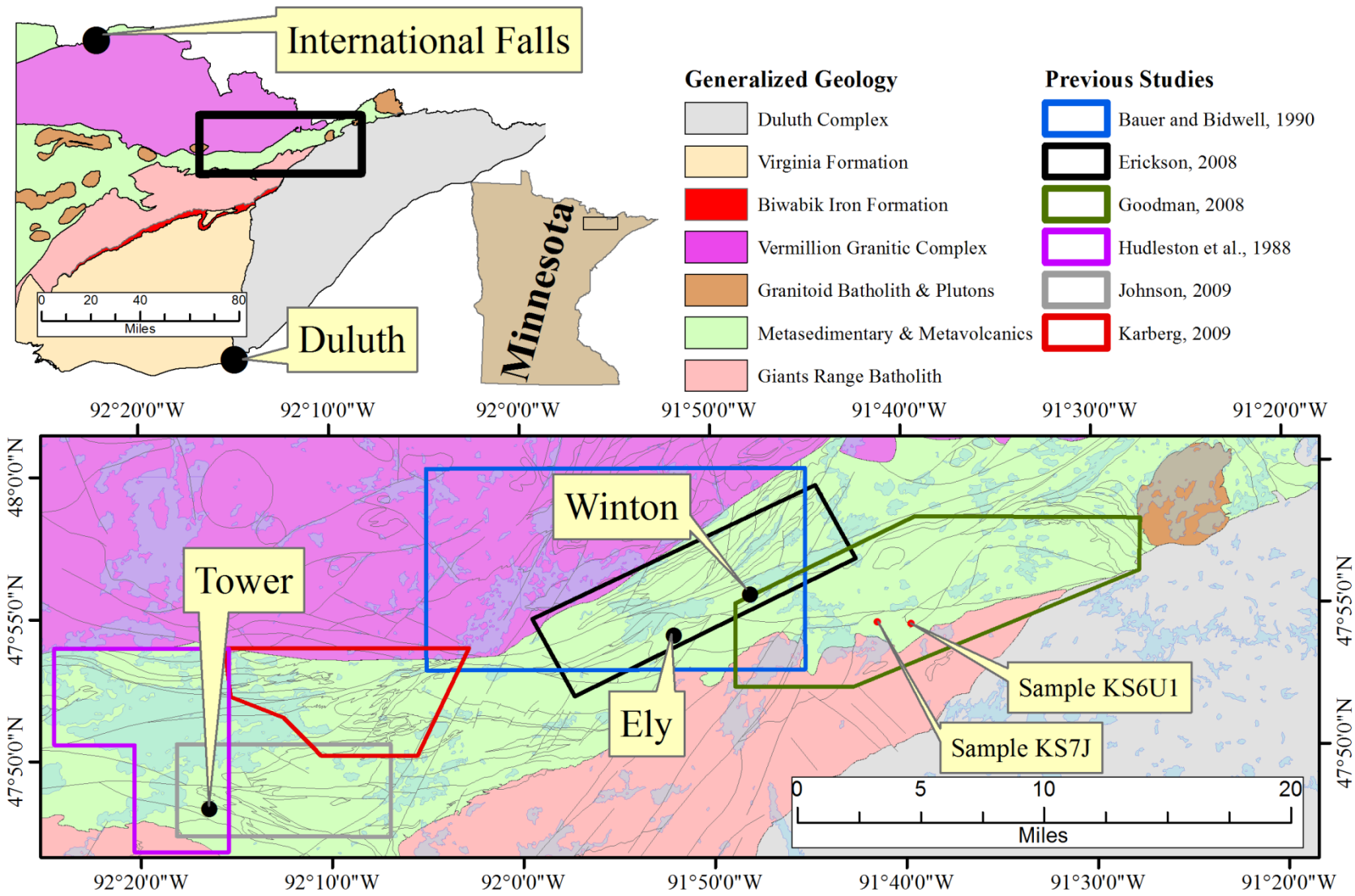

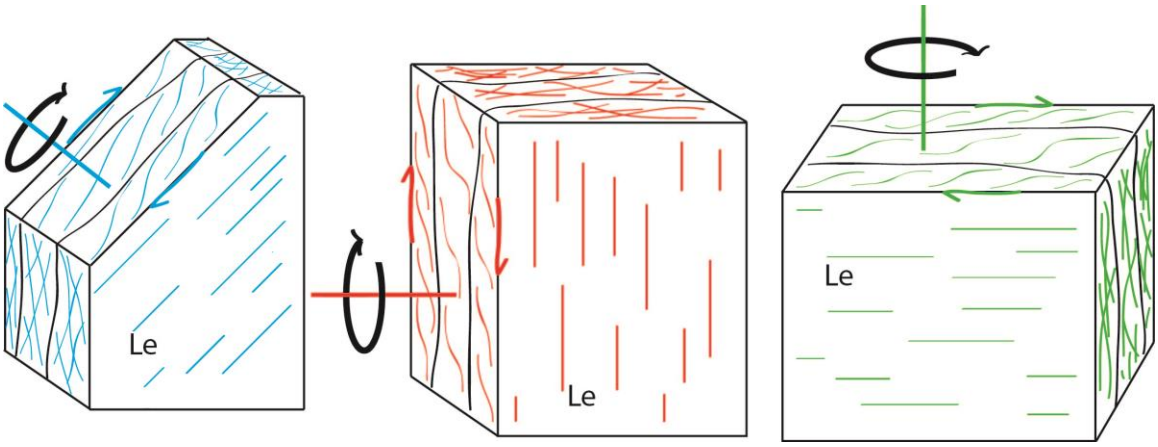

Figure 2. Block diagram displaying shear parallel to the elongation lineation. Note the different orientations of elongation lineation from dominantly vertical and oblique (red/blue) to less commonly horizontal (green). In each case, shear is interpreted to be parallel to the elongation lineation (Goodman, 2008; Erikson, 2008; Karberg, 2009; Johnson, 2009; Goldner, 2013). Based on the asymmetric fabrics, the vorticity vector is inferred to be orientated within the foliation plane, perpendicular to the elongation lineation. Additionally, in the case of oblique elongation lineations (blue), one might expect to observe an apparent asymmetry on the horizontal surface. Kinematic interpretations of this apparent asymmetry are flawed for they are viewed in an arbitrary plane with respect to the elongation lineation.

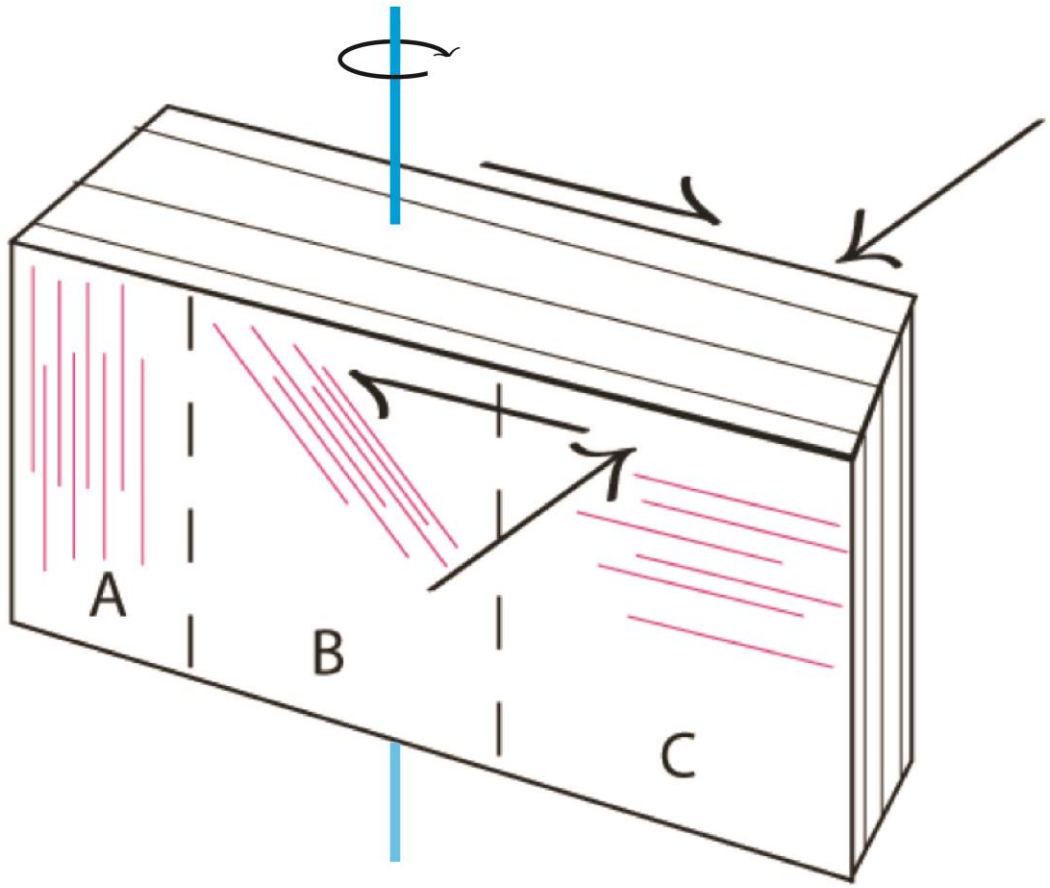

Figure 3. Block diagram displaying dextral transpression hypothesis. This hypothesis invokes shear at varying angles to the elongation lineation ranging from 90˚ (A) to 45˚(B) to parallel (C). A similar geographic orientation of the inferred vorticity axis (blue) is present irrespective of elongation lineation orientation.

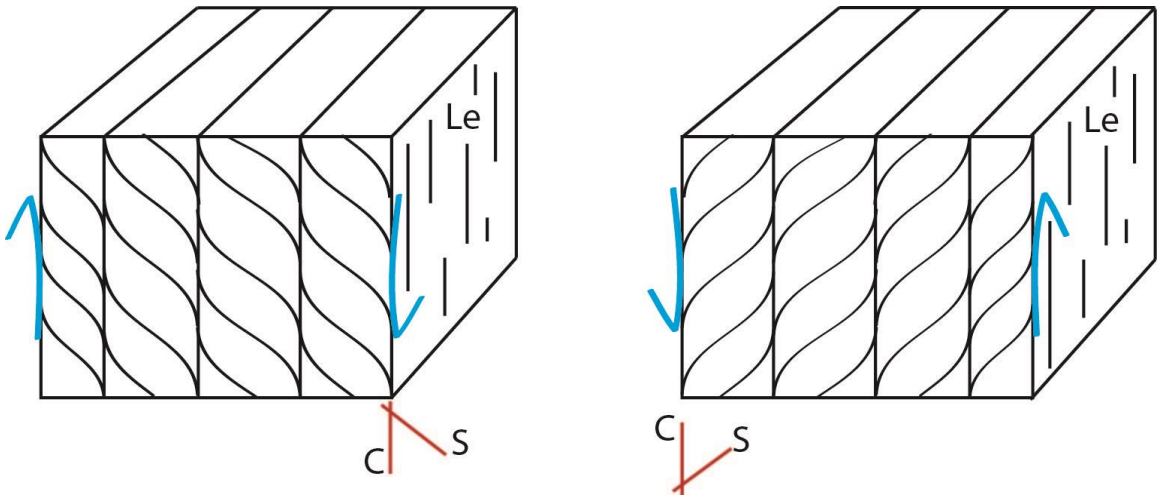

Figure 4. Block diagram of S/C fabric geometry of non-coaxial deformation. S-surfaces form due to the accumulation of finite strain and are cut by C-surfaces. C-surfaces represent zones of high shear strain and form parallel to the shear zone boundary (Berthé et al., 1979; Lister and Snoke, 1984). Note the asymmetric fabric is indicative of shear when viewed in a Le-parallel, Mf-normal plane.

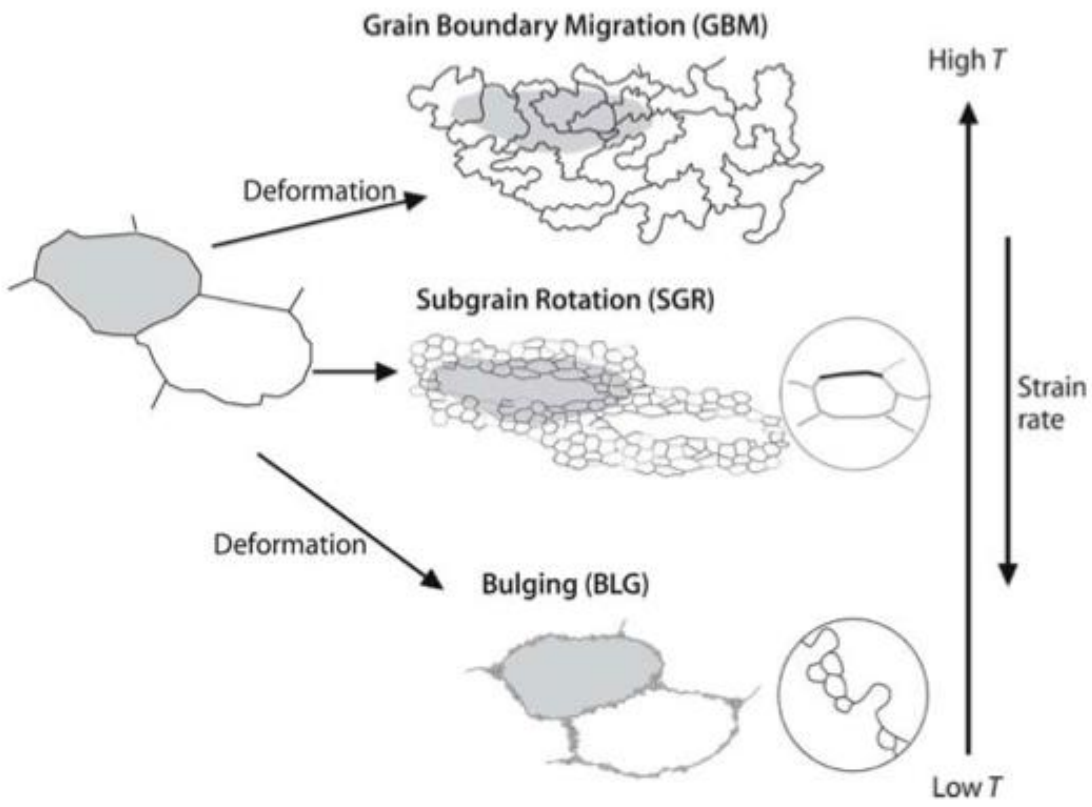

Figure 5. Deformation mechanisms of quartz and general microstructures of resulting recrystallized grains. Shaded grain is the source of the recrystallization. From Passchier and Trouw (2005).

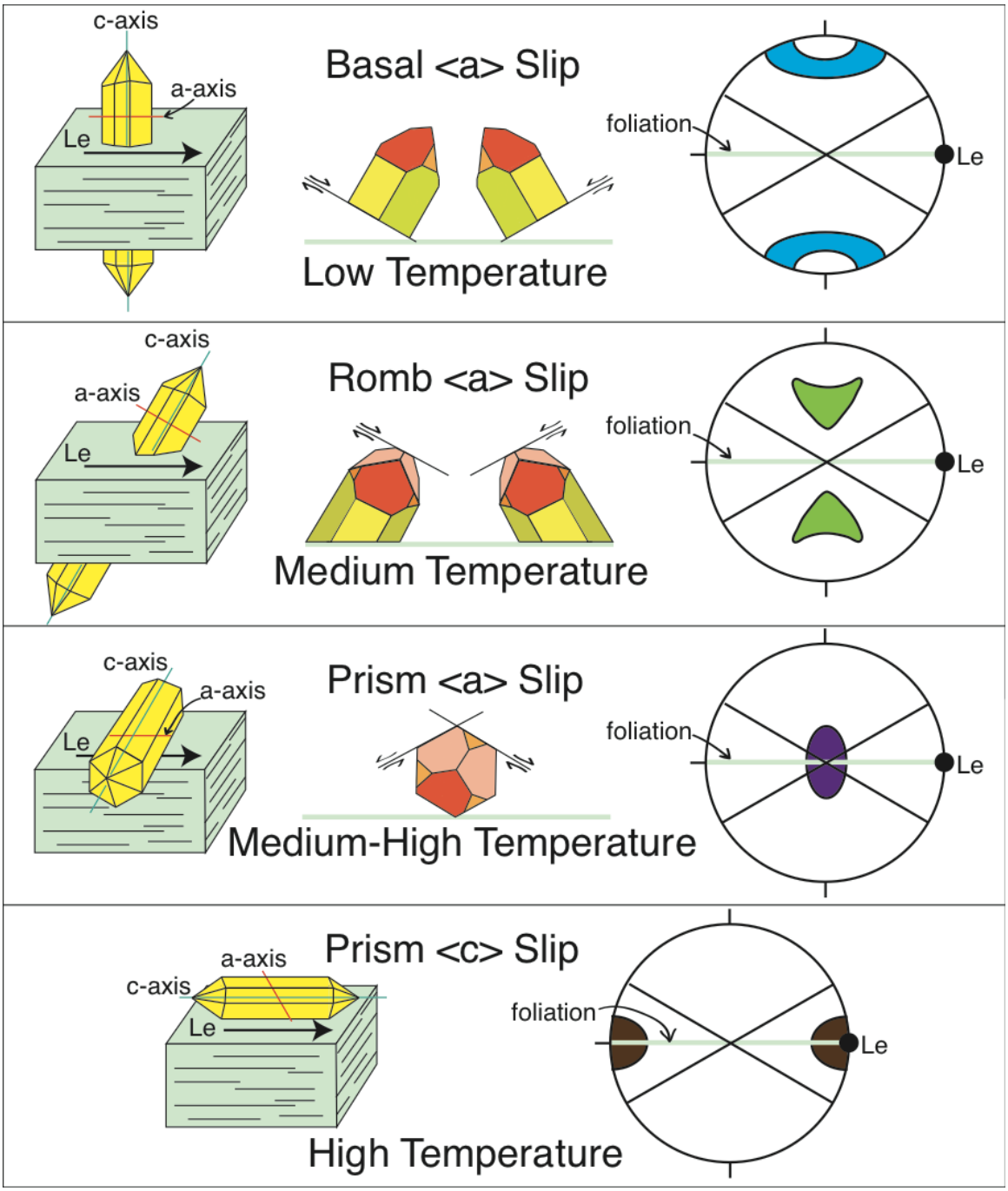

Figure 6. Crystallographic slip systems of quartz. Stereographic projections correspond to c-axis populations as a result of the active slip system, plotted in relation to foliation and elongation lineation (Figure courtesy of D. Oliver).

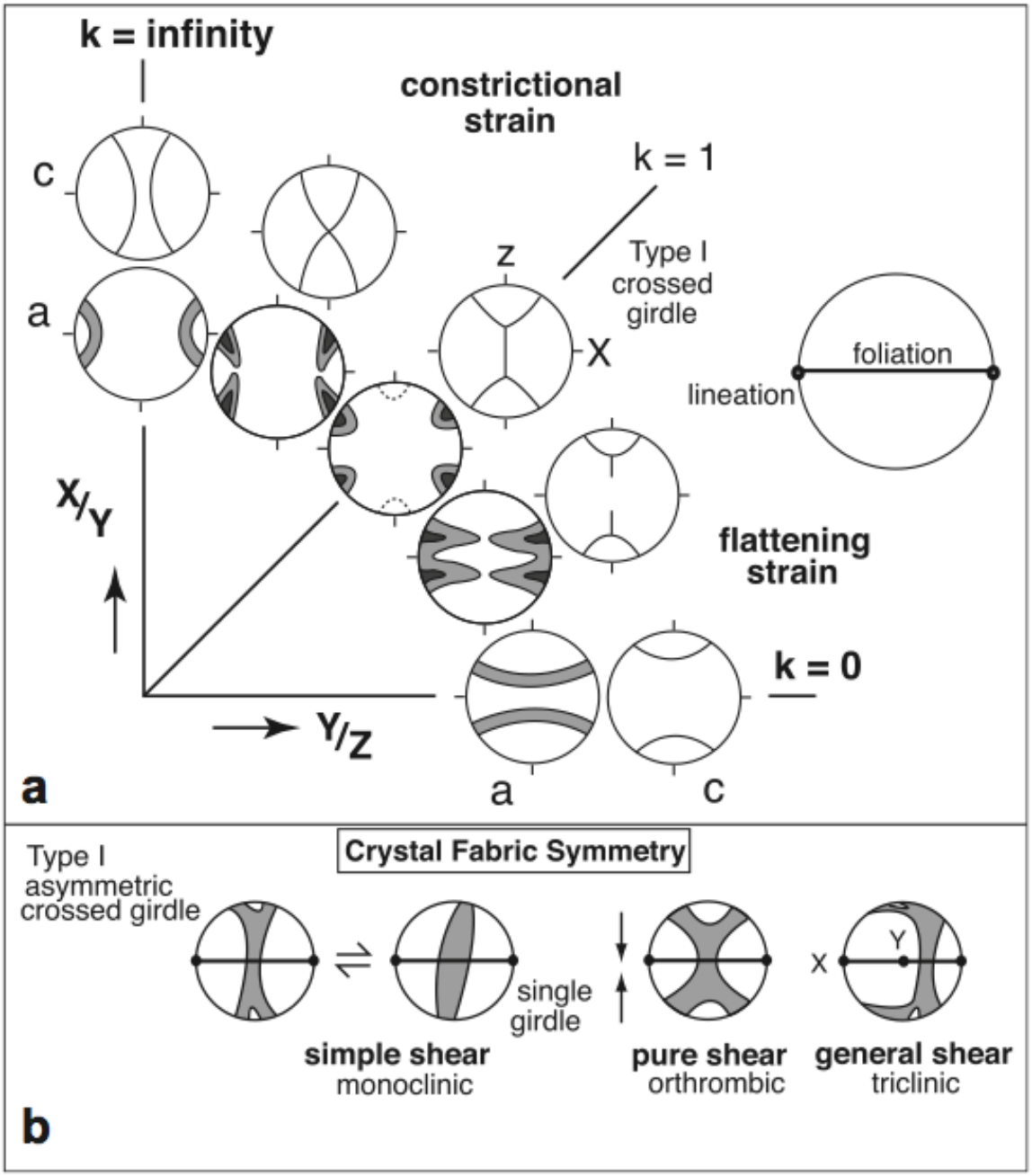

Figure 7a. Quartz *c*- and *a*- axes fabrics of various strain states for coaxial deformation (from Thigpen et. al., 2010; after Schmid and Casey 1986).

Figure 7b. Quartz *c*-axis fabric symmetry. Non-coaxial plane-strain deformation (simple shear) results in Type I asymmetric fabrics. Coaxial-plane-strain deformation (pure shear) results in Type I crossed girdle symmetric fabrics. Non-coaxial non-plane strain (general shear) results in more complex fabric geometry displaying characteristics of both pure and simple shear (from Thigpen et. al., 2010; after Schmid and Casey 1986).

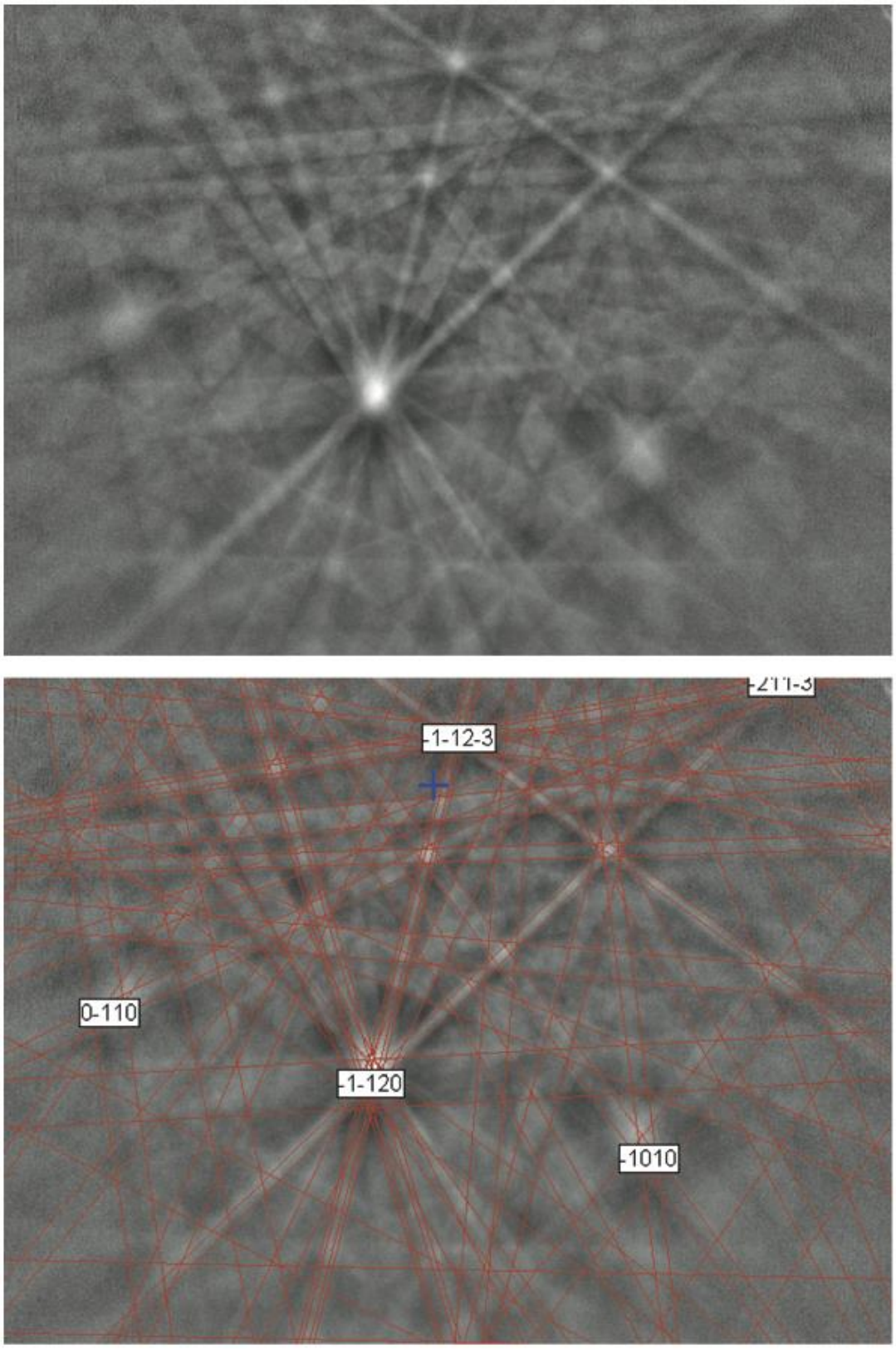

Figure 8. Electron backscatter pattern of quartz produced from sample KS7J. Kikuchi lines are formed by electrons diffracting through lattice planes. Lower image is the indexed pattern.

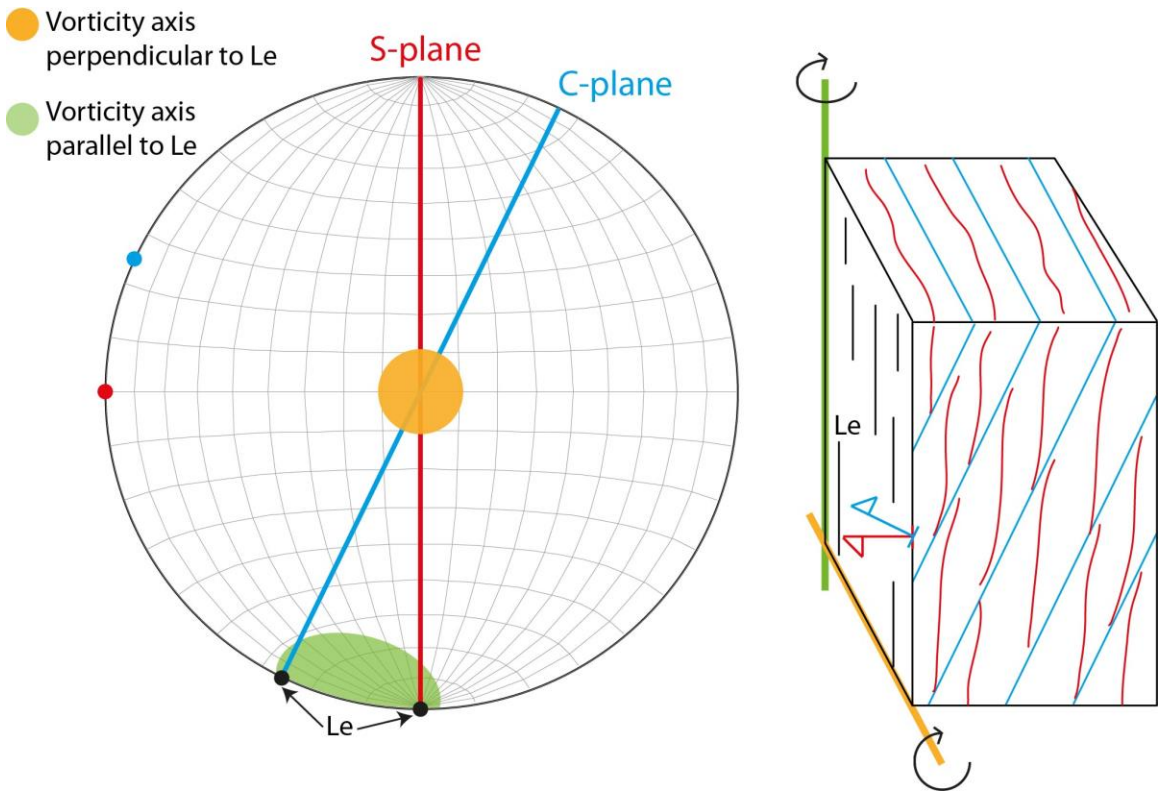

Figure 9. Stereographic and block diagram displaying the spatial relationship between the vorticity axis and elongation lineation. In stereographic view, the vorticity axis and elongation lineations plot as points. The black points represents the elongation lineation (contained within the S- or C-plane). The orange point represents the orientation of the vorticity axis located perpendicular to the elongation lineation. The green area represents the range of orientations of the vorticity axis located parallel to the elongation lineation. For reference the poles to the S- and C- surfaces are represented as red and blue dots respectively.

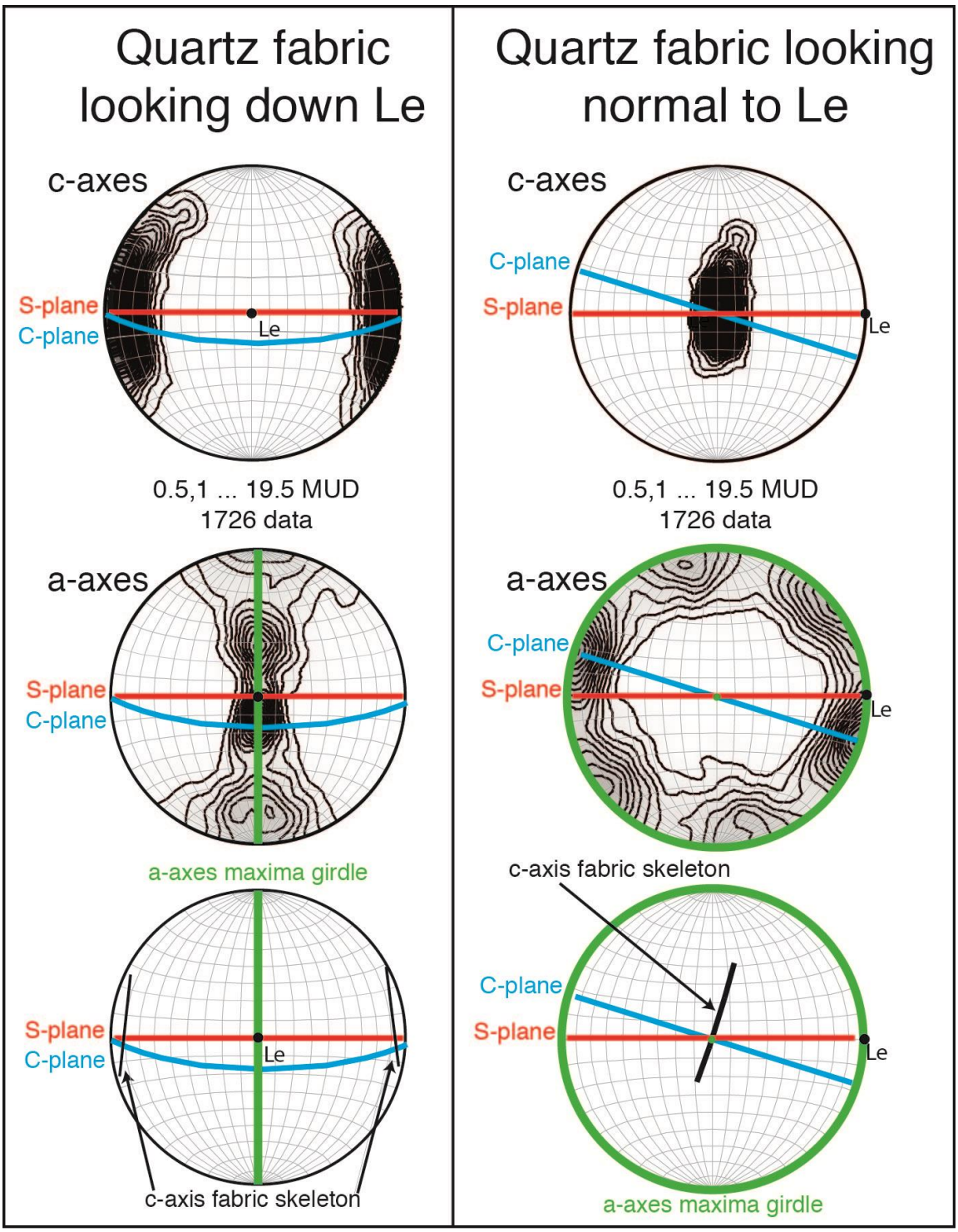

Figure 10. Quartz fabrics of sample KS6U1. Fabrics are viewed looking down the elongation lineation (left) and looking normal to the elongation lineation, parallel to the S/C foliations (right). Symmetric fabrics are present looking down the elongation lineation and asymmetric fabrics are present looking normal to the elongation lineation, parallel to the S/C foliations, indicative of lineation parallel shearing.

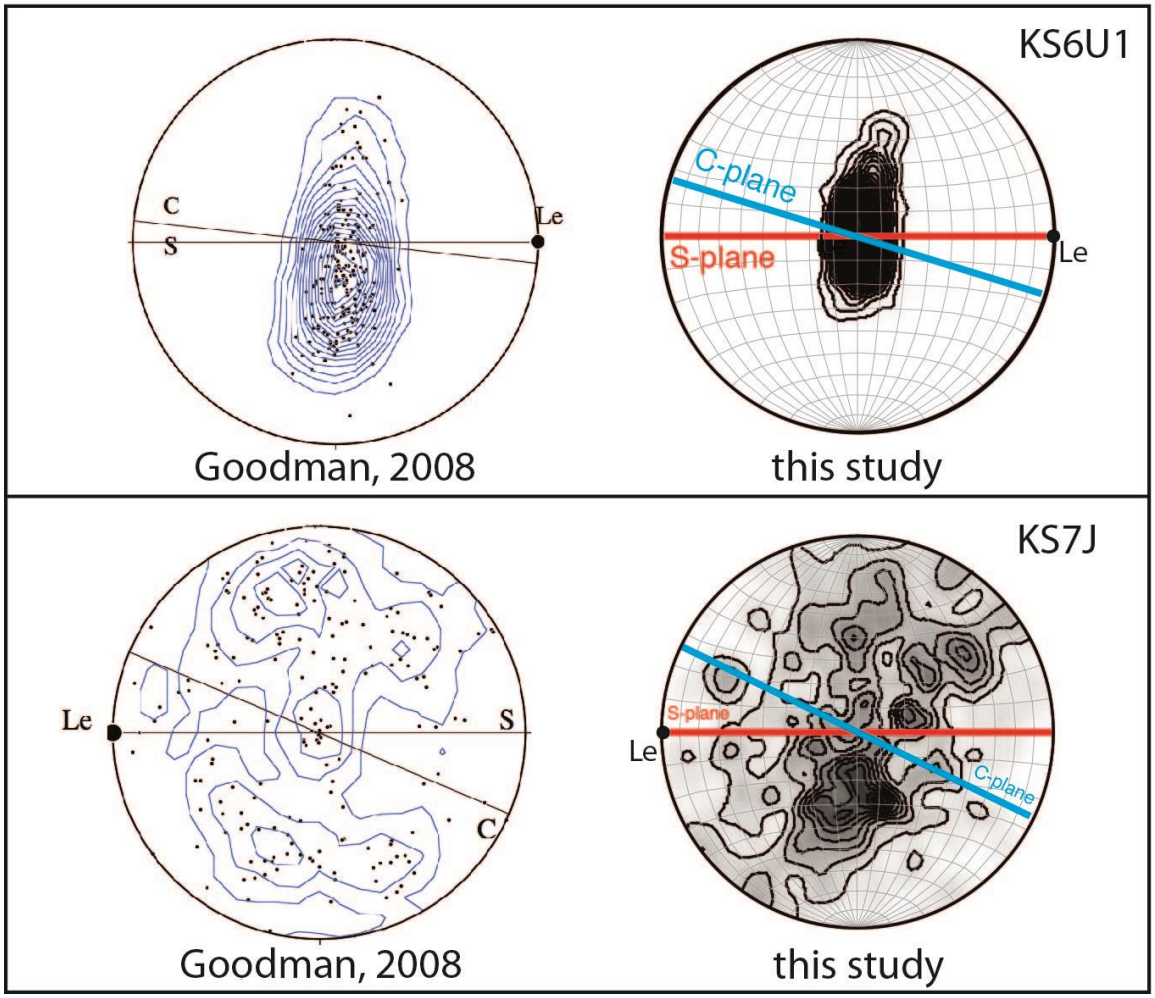

Figure 11. Quartz c-axis fabrics of samples KS6U1 and KS7J from Goodman (2008) and this study. Data from this study display similar fabrics to Goodman (2008).

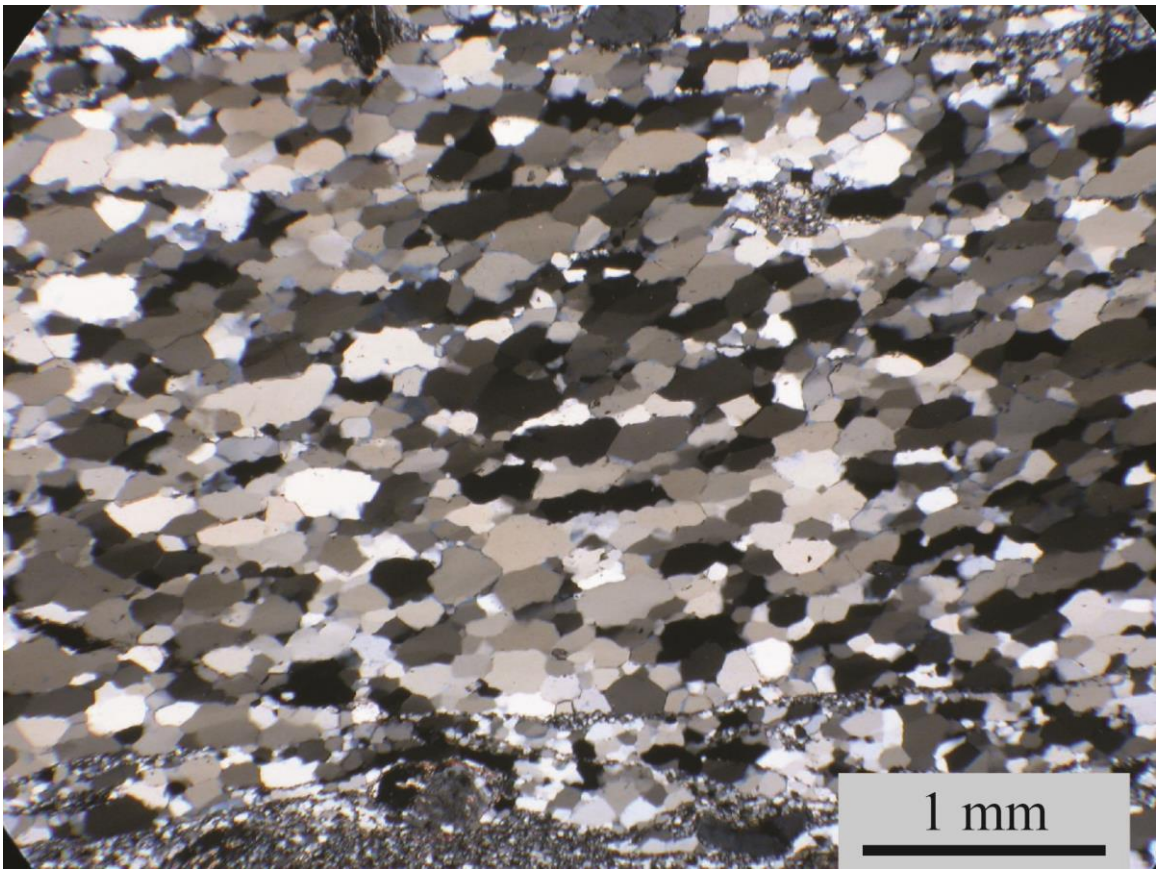

Figure 12. Photomicrograph of sample KS6U1 as viewed in a plane nearly normal to Mf and looking approximately down Le with crossed polarized light. Apparent asymmetry is attributed to the offset of the thin-section to perpendicular Le (15°).

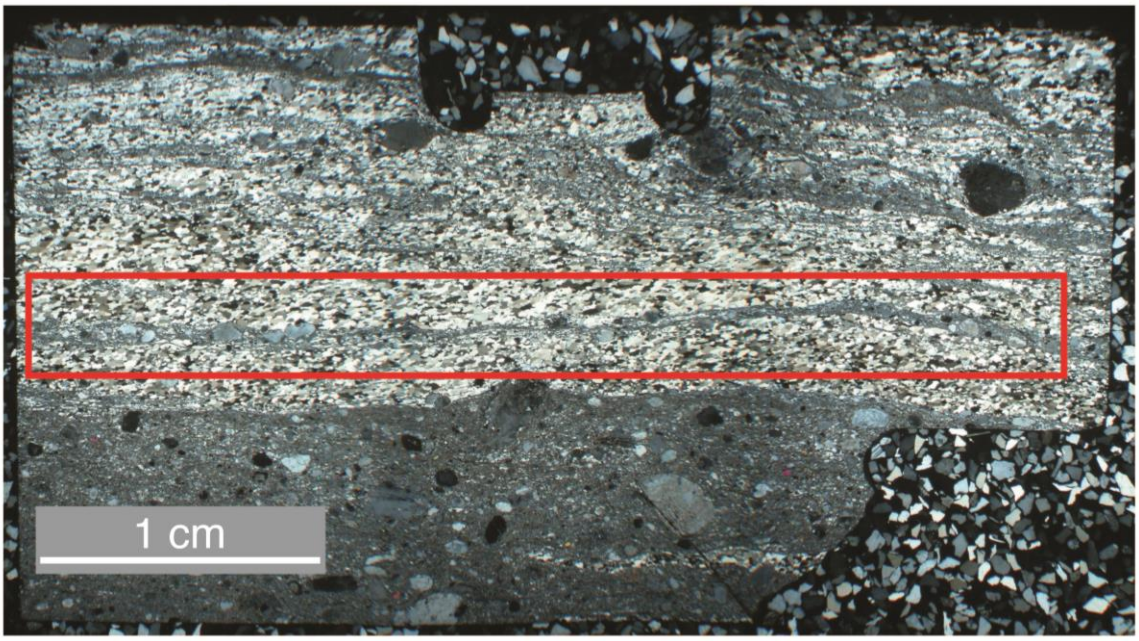

Figure 13. Photomicrograph of sample KS6U1 outlining SEM/EBSD acquisition area (red) as viewed in a plane normal to Mf and looking down Le with crossed polarized light.

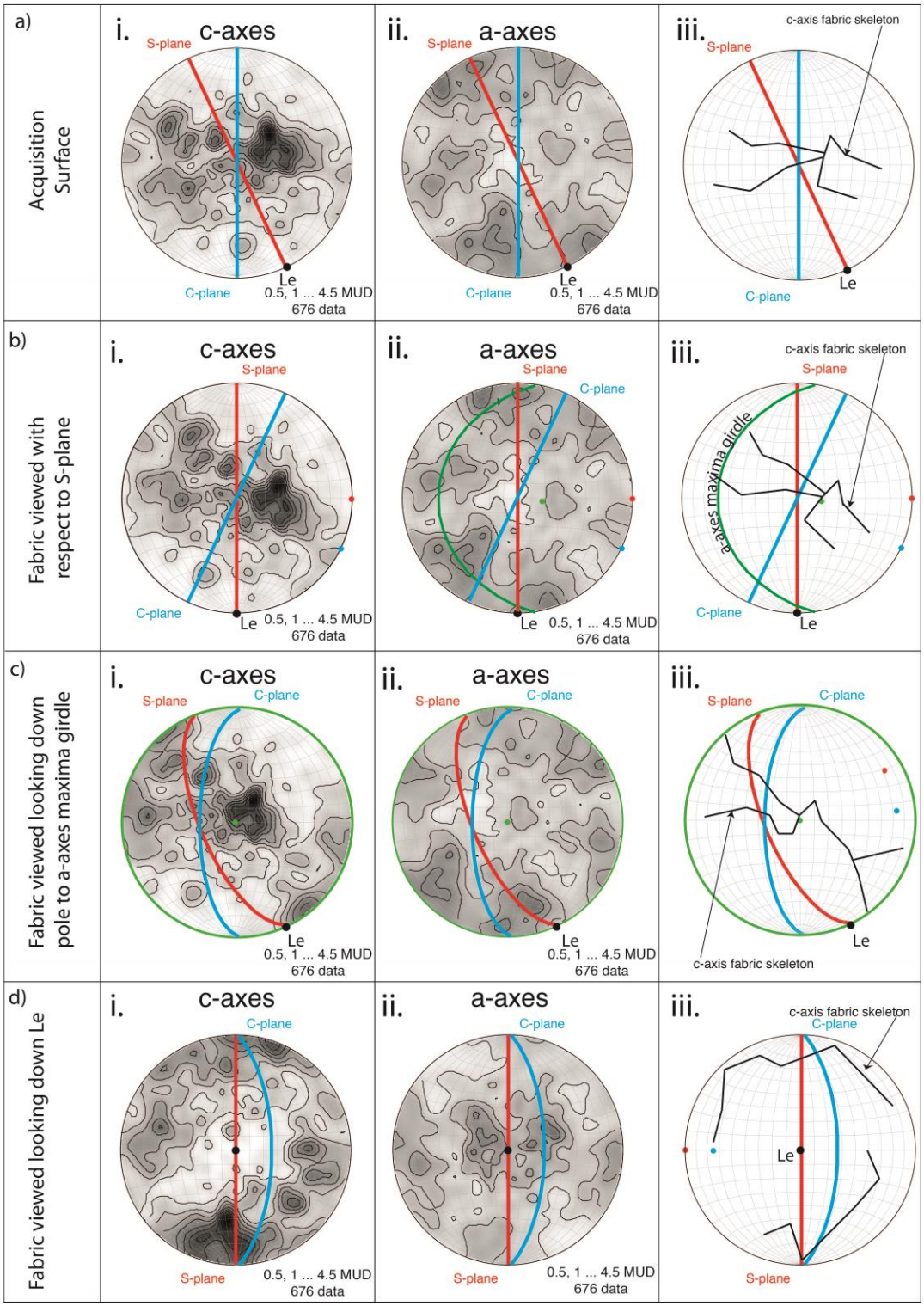

Figure 14. Quartz fabrics of sample KS7J. Each row (a,b,c,d) represent a different view of fabric. Fabric skeleton are provided within each view. Asymmetric fabrics are present when a plane normal to the s-foliation and containing the elongation lineation (row b) imply shear sense (right lateral; north-side up). The vorticity vector is interpreted to be the pole to the a-axes maxima girdle. When viewed looking down the pole to the a-axes maxima girdle, asymmetric fabrics are present (row c). Furthermore, when viewed looking down the elongation lineation, symmetric fabrics are present (row d).

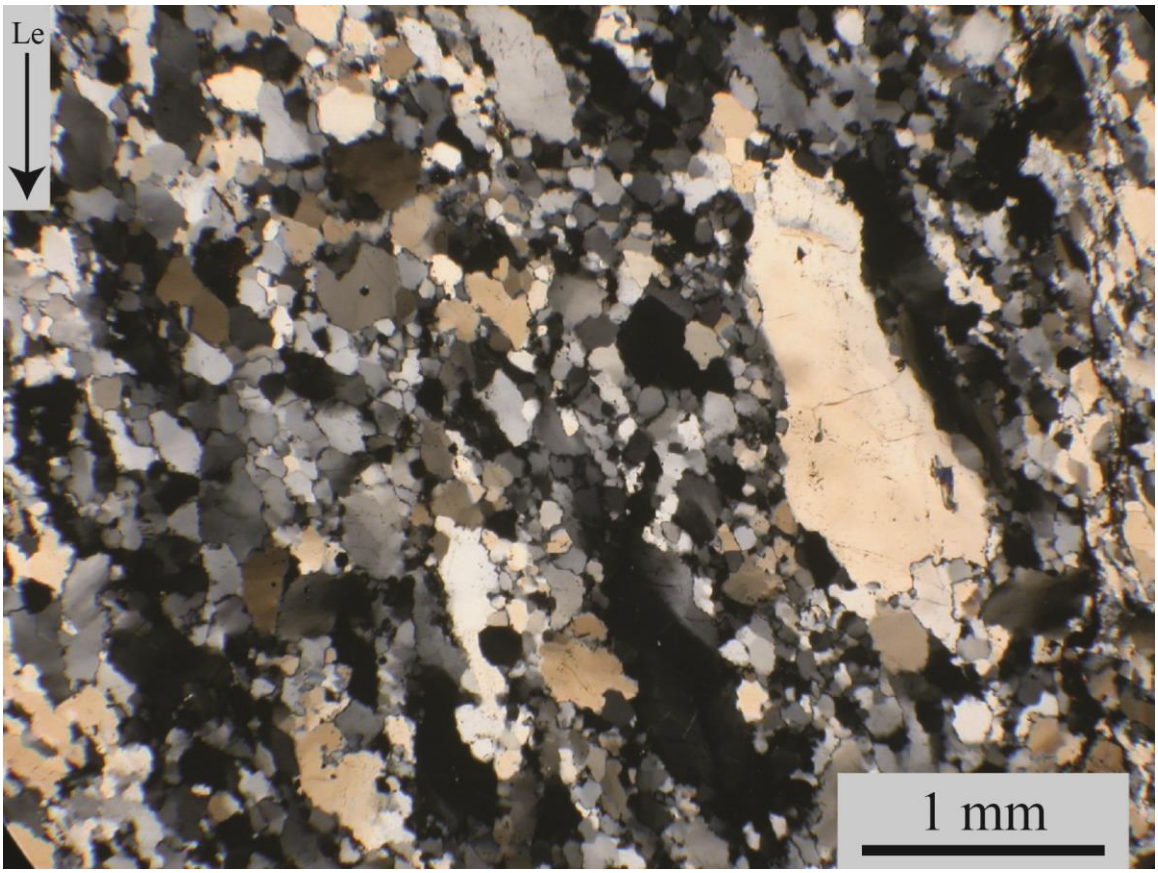

Figure 15. Photomicrograph of sample KS7J. This is an Le-parallel, Mf-normal view; crossed polarized light.

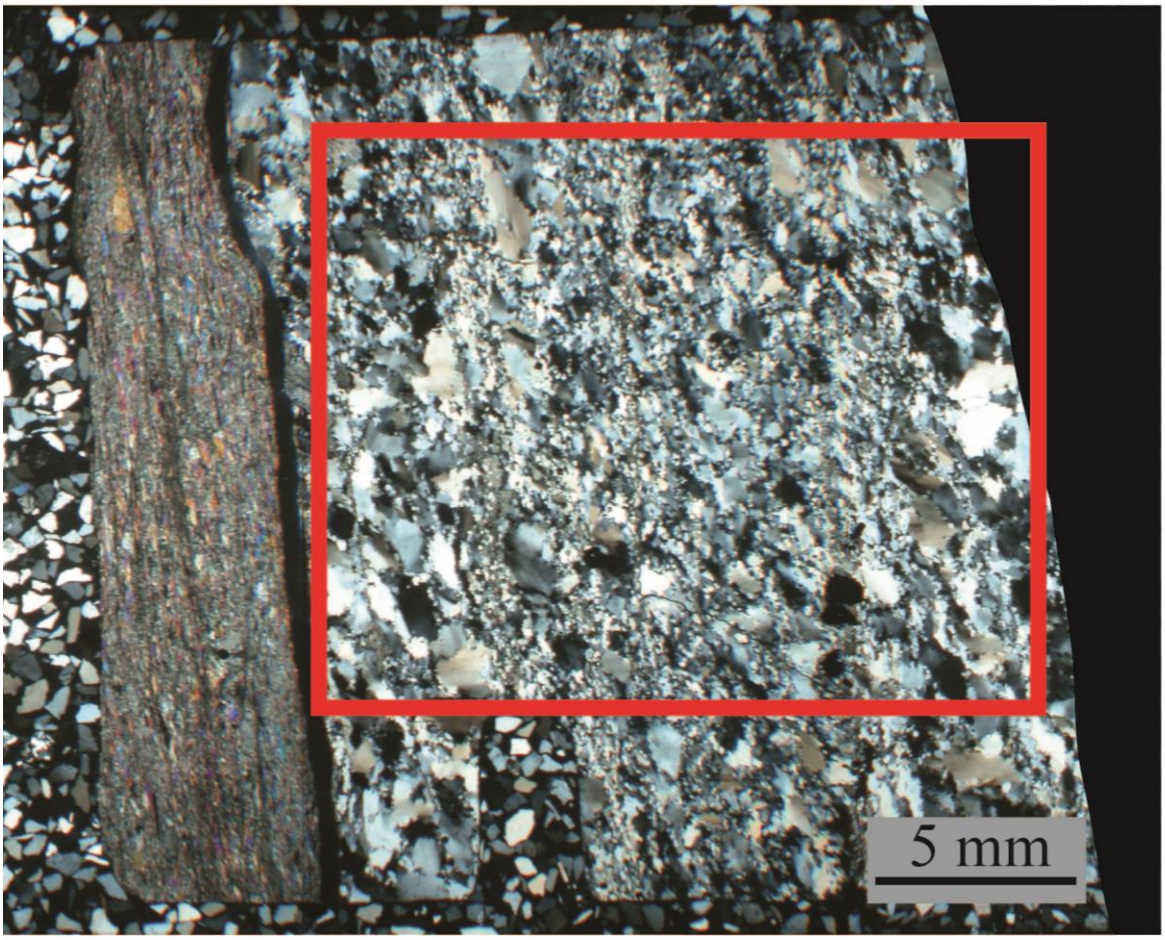

Figure 16. Photomicrograph of sample KS7J outlining SEM/EBSD acquisition area (red) as viewed in a an Le-parallel, Mf-normal view with crossed polarized light.

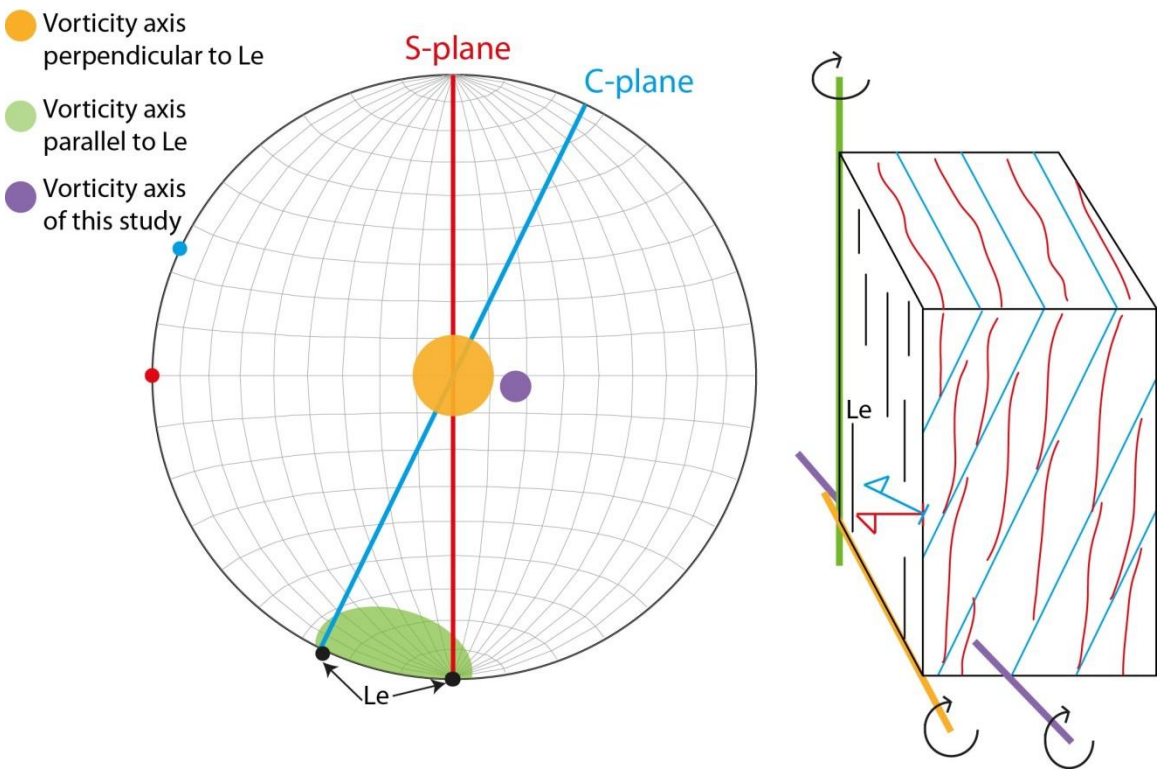

Figure 17. Stereographic and block diagram displaying the vorticity axis of the dip-parallel sample KS7J. The vorticity axis of this study (purple) is oriented near 90° from the elongation lineation.

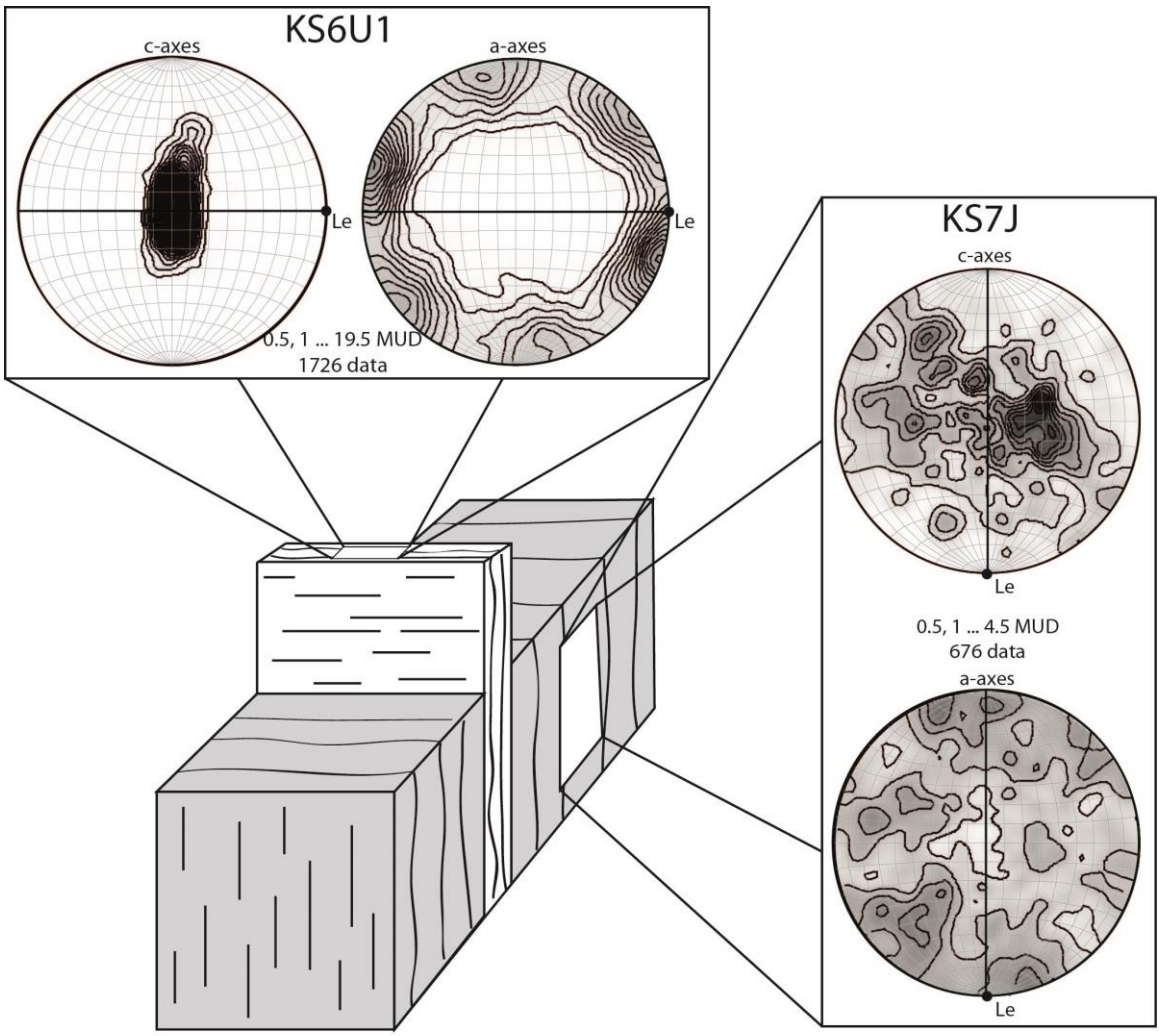

Figure 18. Cartoon block diagram of the Kawishiwi shear zone displaying relationship between dominate dip-parallel Le (grey) and localized strike-parallel Le (white). Localized strike-parallel zones are narrow and often sharply bounded by the pervasive dip-parallel fabrics. Quartz fabrics of this study are also illustrated.

References:

Bauer, R.L., and Bidwell, M.E., 1990, Contrasts in the response to dextral transpression across the Quetico-Wawa subprovince boundary in northeastern Minnesota: Canadian Journal of Earth Sciences, v. 27, p. 1521-1535.

Berthé, D., Choukroune, P., and Jegouzo, P., 1979, Orthogneiss, mylonite and non-coaxial deformation of granite: the example of the South Armoricain shear zone: Journal of Structural Geology, v. 1, p. 31-44.

Clements, J. M., 1903, The Vermilion iron-bearing district of Minnesota: United States Geological Survey Monograph, v. 45, 463 p.

Drury, M.R., Humphreys, F.J., and White, S.H., 1985, Large strain deformation studies using polycrystalline magnesium as a rock analogue. Part II: dynamic recrystallization mechanisms at high temperatures: Physics of the Earth and Planetary Interiors, v. 40, p. 208-222.

Erikson, E.J., 2008, Structural and Kinematic Analysis of the Shagawa Lake Shear Zone, Superior Province, Northeastern, Minnesota: Implications for Archean (2.75 Ga) Crustal Evolution [M.S. thesis]: Duluth, University of Minnesota, 65 p.

Erikson, E.J., 2010, Structural and kinematic analysis of the Shagawa Lake shear zone, Superior Province, northern Minnesota: implications for the role of vertical versus horizontal tectonics in the Archean: Canadian Journal of Earth Sciences, v. 47 no. 12, p. 1463-1479.

Goldich, S.S., 1972, Geochronology in Minnesota, *in* Sims, P.K., and Morey, G.B., ed., Geology of Minnesota: A Centennial Volume: Minnesota Geological Survey, p. 27-37.

Goldner, J. N., 2013, Structure and metamorphism along the Burntside Lake Shear Zone near Ely, Minnesota [M.S. thesis]: Duluth, University of Minnesota, 92 p.

Goodman, S.K., 2008, Structural and kinematic analysis of the Kawishiwi shear zone, Superior Province: Insight on granite-greenstone terrain tectonics and Archean (2.7 Ga) crustal evolution [M.S. thesis]: Duluth, University of Minnesota, 82 p.

Gruner, J.W., 1941, Structural geology of the Knife Lake area of northeaster Minnesota: Geological Society of America Bulletin, v. 52. P. 1577-1642.

Hansen, V.L., 1990, Collection and preparation of thin sections of orientated samples: Journal of Geologic Education, v. 38, p. 294-297.

Hirth, G., Tullis, J., 1992, Dislocation creep regimes in quartz aggregates: Journal of Strcutral Geology, v. 14 no. 2, p. 145-159.

Hooper, P.R., and Ojkangas, R.W., 1971, Multiple deformation in Archean rocks of the Vermilion District, Northeastern Minnesota: Canadian Journal of Earth Sciences, v. 8, p. 423-434.

Hudleston, P.J., 1976, Early deformational history of Archean rocks in the Vermilion District, Northeastern Minnesota: Canadian Journal of Earth Sciences, v. 13, p. 579-592.

Hudleston, P.J., Schultz-Ela, D., and Southwick, D.L., 1988, Transpression in an Archean greenstone belt, northern Minnesota: Canadian Journal of Earth Sciences, v. 25, p. 1060-1068

Jirsa, M.A., Southwick, D.L., and Boerboom, T.J., 1992, Structural evolution of Archean rocks in the western Wawa subprovince, Minnesota: refolding of precleavage napps during D2 transpression: Canadian Journal of Earth Sciences, v. 29, p. 2146-2155.

Jirsa, M.A., Boerboom, T.J., Chandler, V.W., Mossler, J.H., Runkel, A.C., and Setterholm, D.R., 2011, Geologic Map of Minnesota-Bedrock Geology: Minnesota Geological Survey Slate Map Series S-21, scale 1:500 000, 1 sheet, 10 p. text.

Johnson, T.K., 2009, Structural, Kinematic, and Hydrothermal Fluid Investigation of the Gold-Bearing Murray Shear Zone, Northeastern Minnesota [M.S. thesis]: Duluth, University of Minnesota, 143 p.

Karberg, S.M., 2009, Structural and Kinematic Analysis of the Mud Creek Shear Zone, Northeastern Minnesota [M.S. thesis]: Duluth, University of Minnesota, 70 p.

Law, R.D., 1990, Crystallographic fabrics: a selective review of their applications to research in structural geology, *in* Knipe, R.J., and Rutter, E.H., ed., Deformation Mechanisms, Rheology and Tectonics: Geological Society of London Special Publications, v. 54, p. 335-352.

Lin, S., Jiang, D., and Williams, P.F., 2007, Importance of differentiating ductile slickenside striations from stretching lineations and variation of shear direction across a high-strain zone: Journal of Structural Geology, v. 29, p. 850-862.

Lin S., and Williams, P.F., 1992, The origin of ridge-in-groove slickenside striae and associated steps in an S-C mylonite: Journal of Structural Geology, v. 14, p. 315-321.

Lister, G.S., and Hobbs, B.E., 1980, The simulation of fabric development during plastic deformation and its application to quartzite: the influence of deformation history: Journal of Structural Geology, v. 2 no. 3, p. 355-370.

Lister, G.S., and Snoke, A.W., 1984, S-C Mylonites: Journal of Structural Geology, v. 6 no. 6, p. 617-638

Oliver, D., 1996, Structural, Kinematic and Thermochronometric Studies of the Teslin Suture Zone, South-Central Yukon Territory [Ph.D. thesis]: Southern Methodist University, 231 p.

Ojkangas, R.W., 1972, Archean Volcanogenic Graywackes of the Vermilion District, Northeastern Minnesota: Geological Society of America Bulletin, v. 83 no.2, p. 429-442.

Passchier, C.W., and Trouw, R.A.J., 2005, Micro-tectonics: Springer, 366 p.

Schmid, S.M., and Casey, M., 1986, Complete fabric analysis of some commonly observed quartz c-axis patterns, *in* Hobbs, B.E., Heard, H.C., ed., Mineral and Rock

Deformation Laboratory Studies: The Paterson Volume, Geophysical Monograph 36, American Geophysical Union, p. 263-286.

Schultz-Ela, D.D., and Hudleston, P.J., 1991, Strain in an Archean greenstone belt of Minnesota: Tectonophysics, v. 190, p. 233-268.

Shigematsu, N., 1999, Dynamic recrystallization in deformed plagioclase during progressive shear deformation: Tectonophysics, v. 305, p. 437-452.

Sims, P.K., 1972, Northern Minnesota, Vermilion District and Adjacent Areas, *in* Sims, P.K., and Morey, G.B., ed., Geology of Minnesota: A Centennial Volume: Minnesota Geological Survey, p. 49-62.

Sims, P.K., 1976, Early Precambrian tectonic-igneous evolution in the Vermilion district, northeastern Minnesota: Geological Society of America Bulletin, v. 87, p. 379-389.

Sims, P.K., and Southwick, D.L., 1985, Geologic Map of Arcehan rocks, western Vermilion district, northern Minnesota: United States Geological Survey, Miscellaneous Investegations Map I-1527m scale 1:48 000, 1 sheet.

Stipp, M., Stunitz, H., Heilbronner, R., Schmid, S., 2002b. Dynamic recrystallization of quartz: correlation between natural and experimental conditions. In: De Meer, S., Drury, M.R., De Bresser, J.H.P., Pennock, G.M. (Eds.), Deformation Mechanisms, Rheology and Tectonics: Current Status and Future Perspectives: Geological Society of London Special Publications, v. 200, p. 171-190.

Thigpen, J.R., Law, R.D., Llyod, G.E., and Brown. S.J., 2010, Deformation temperatures, vorticity of flow, and strain in the Moine thrust zone and Moine nappe: Reassessing the tectonic evolution of the Scandian forland-hinterland transition zone: Journal of Structural Geology, v. 32, p. 920-940.